AIAA SciTech Forum
8-12 January 2024, Orlando, FL
AIAA SCITECH 2024 Forum

10.2514/6.2024-0787

A Generalized Continuous Mesh Framework for Explicit Mesh Curving

Lucien Rochery*, Marshall C. Galbraith†, David L. Darmofal‡, Steven R. Allmaras§
Massachusetts Institute of Technology, Cambridge, MA, 02139

This paper proposes a new generalization of the continuous mesh framework to high-order (curved) meshes. In the classic linear framework, unit elements in a metric field, by definition, have edge lengths of one. However, this definition of unity is not sufficient to define the shape (Jacobian matrix everywhere) of high-order elements. We propose a generalization to high-order elements that prescribes the element Jacobian matrix everywhere, as well as higher order derivatives. Applying this to P^2 simplices, we obtain explicit geometric relationships to curve unit elements in one step. Simple numerical examples show meshes curved in this manner have edges following dominant metric directions. Some theoretical results can also be shown. As h goes to 0, elements become straighter at the rate expected to preserve interpolation error convergence. The discrete unit definition (analogous to unitness in a single metric in the linear case) can be relaxed to a fully continuous one. We illustrate a use of this in generalizing the classic multi-scale error estimate to high-order meshes, a metric-based error estimate of the L^p norm of interpolation error.

I. Introduction

Metric-based mesh adaptation relies on metric fields to prescribe mesh element sizes and shapes. A uniform mesh is constructed, but with distance and angle computations modified according to an input metric field $\mathcal{M}$. Such metric fields are usually produced by minimizing an error estimator, whether a priori [1, 2] or a posteriori [3–6]. These estimators can be derived because an element is unit in a single metric, which is given explicitly by the element Jacobian. Metric fields have been derived to control various errors, such as geometric accuracy of the surface mesh, interpolation error L^p norms, or functionals of solution fields (e.g. drag, lift). As a result, metric-based mesh adaptation on linear meshes has been applied successfully to a great range of physical phenomena and error estimators [7–12]. This framework has been extended to high-order discretizations on linear meshes [13].

Curved elements for the Finite Element Method (FEM) were considered as early as the 60s [14]. Isoparametric finite elements could be found in textbooks by the end of the 70s [15]. Most common numerical methods (DG, BEM, Finite Volumes) have been extended to use curved Bézier meshes since then. The optimal scheme degree for several DG-like methods is shown theoretically [16] to be greater than one, especially for lower target errors and in 3D. Order 3 methods are shown to provide optimal error over work ratio in an empirical study representing a wide range of complex CFD applications [17]. However, these high-order numerical methods require high-order (curved) meshes to conserve their advantageous properties. Physical features may be lost due to piece-wise linear surfaces [18] and optimal convergence may require a curved boundary [19, 20]. In some cases, it might even be necessary to represent the geometry with curved elements of a higher polynomial degree than the solution [21].

Despite this, high-order mesh generation has not yet reached a degree of maturity comparable to linear meshing, and still presents a number of major challenges, both theoretical and practical. Curving boundary elements also requires curving domain-interior elements to guarantee mesh validity, thus meshes with curved boundaries must be curved everywhere. In the worst case, interpolation error for degree q curved elements can lead to order $\lfloor p/q \rfloor + 1$ convergence rates instead of the expected order $p + 1$ [22, 23]. Beyond preserving error convergence rates, these additional element degrees of freedom must be harnessed to further minimize error at fixed computational cost, much like anisotropy is used in adaptation. Super-convergence due to domain-interior element curvature is observed in [24] for boundary approximation, in [25] for interpolation error (several degrees) in 2D, and in [26] for P^2 interpolation error in 3D. Except for boundary approximation in [24], these have been empirical numerical studies.

*PostDoctoral Associate, Department of Aeronautics & Astronautics, AIAA Member
†Research Engineer, Department of Aeronautics & Astronautics, AIAA Senior Member
‡Professor, Department of Aeronautics & Astronautics, AIAA Fellow
§Research Engineer, Department of Aeronautics & Astronautics, AIAA Associate Fellow

Developments on metric-based high-order meshing have been as follows. In [27, 28], interpolation error is integrated along mesh edges in 2D, leading to a simplified a priori metric-based error estimate involving curvilinear edge length, which is minimized. Edge length minimization is similarly used in [29] as a comparatively fast curvature driver in 3D. In [30], a metric-based distorsion measure is generalized to high-order elements and used to produce curved meshes in 2D and 3D. This is an algebraic generalization, so to speak, which implicitly enforces a definition of high-order metric conformity formally $\mathcal{J}_K \sim \mathcal{M}^{-1/2}$. In [31], MOESS is extended to high-order elements, assuming a mesh-implied metric also formally $\mathcal{J}_K \sim \mathcal{M}^{-1/2}$.

In this article, we seek to formalize a unit relationship (formally $\mathcal{J}_K \sim \mathcal{M}^{-1/2}$) from the basic principles of metric-based adaptation, namely that the metric field describes local space deformations under which the mesh should be uniform (isotropic). We start with a discrete analysis, by looking for the simplest type of metric field that can prescribe any quadratic simplex, in a manner that is consistent with the linear case (i.e. if $\mathcal{M}$ is constant, then any element unit in $\mathcal{M}$ must be linear). This is by analogy with studying elements unit in a single metric (rather than metric field) in the linear case. Explicit formulas for unit control point locations are derived. If the subjacent linear element is already unit, this produces a unit quadratic simplex in one simple step. Although mesh mechanics are not the focus on this paper, some basic curving results are shown to illustrate the kind of curvature these geometric relationships prescribe. Next, we consider embedded metric field families $(\mathcal{M}_h = h^{-2}\mathcal{M})_{h>0}$ and show some basic asymptotic estimates, namely that elements unit in $\mathcal{M}_h$ have $O(h^2)$ second derivatives. This means unit meshes are regular in the sense of [32] regardless of the base metric field $\mathcal{M}$ and interpolation error convergence rate is as on linear meshes: the subpar convergence rates observed in [22, 23] are automatically avoided. We then show that the discrete definition can be relaxed to a fully continuous one, and with arbitrary (not polynomial) metric fields. Finally, that an element defines a unique implied metric field. These two facts together allow to replace mapping derivatives anywhere by quantities depending on the locally implied metric and derivatives. Use of this is illustrated by deriving an a priori interpolation error estimate, which can be expressed solely as a function of the metric field representing a mesh.

Section II introduces the basic concepts used in this paper. Section III generalizes the unit element definition in a constant metric to the high-order case. The considered metrics may no longer be constant, but not yet fully arbitrary. This allows for an exact discrete analysis. Elementary asymptotic properties of unit elements are given, which allow relaxing the above definition to arbitrary metric fields, up to negligible errors, thus completing the continuous mesh definition. Section IV studies P^2 triangles and tetrahedra in detail, offering explicit formulas for high-order node positioning ensuring elements are unit under the metric in the high-order sense. Some numerical examples are given. Section V illustrates the theoretical uses of this framework by generalizing the metric-based multi-scale (L^p interpolation error norm) estimator [2] to curved meshes, in the elementary case of P^1 interpolation. This completes the justification for these definitions: they are practical both from a meshing and from an error estimation standpoint.

II. Fundamentals

A. The continuous mesh framework

Metrics A metric is a s.p.d. matrix $\mathcal{M}$ that induces a scalar product $\langle \cdot, \cdot \rangle_{\mathcal{M}}$ and Euclidean norm $\| \cdot \|_{\mathcal{M}}$. $\mathcal{M}$ decomposes as $\mathcal{M} = PDP^T$, where the columns of P form an orthonormal basis of $\mathbb{R}^n$ and D is a diagonal matrix of eigenvalues of $\mathcal{M}$. The power function $\mathcal{M}^s = PD^sP^T$ is uniquely defined for all s and coincides with the usual algebraic power for integer s. Of interest is the power $-1/2$ of $\mathcal{M}$ as the unit ball $\mathcal{B}_{\mathcal{M}}(0, 1)$ for the norm $\| \cdot \|_{\mathcal{M}}$ verifies

$$\mathcal{B}_{\mathcal{M}}(0, 1) = \mathcal{M}^{-1/2}\mathcal{B}(0, 1) \tag{1}$$

with $\mathcal{B}(0, 1)$ the unit ball for the usual norm $\| \cdot \|$. Indeed, for all $x \in \mathcal{B}(0, 1)$,

$$\|\mathcal{M}^{-1/2}x\|^2_{\mathcal{M}} = x^T\mathcal{M}^{-1/2}\mathcal{M}\mathcal{M}^{-1/2}x = x^Tx = 1. \tag{2}$$

Thus $\mathcal{M}^{-1/2} : (\mathbb{R}^n, \langle \cdot, \cdot \rangle) \to (\mathbb{R}^n, \langle \cdot, \cdot \rangle_{\mathcal{M}})$ is an isometry and the unit ball for $\mathcal{M}$ an ellipsoid. Denoting λ_i as the eigenvalues of $\mathcal{M}$, the principal axes of the ellipsoid have length $h_i = \lambda_i^{-1/2}$ in the usual norm $\| \cdot \|$, and the axes are the eigenvectors of $\mathcal{M}$ (or columns of P). These are the characteristic sizes and directions implied by the metric.

Unit elements A simplex K, by definition, is unit in a metric $\mathcal{M}$ if its edges are all length 1 for $\| \cdot \|_{\mathcal{M}}$. There exists only one metric in which a given element is unit. This is called its intrinsic or implied metric. A single metric, however, defines a family of unit elements. If K_0 is any regular (equilateral in the usual sense) simplex and R is a rotation matrix,

then $K = \mathcal{M}^{-1/2} RK_0$ is unit in $\mathcal{M}$. Indeed, RK_0 is unit for the usual norm and $\mathcal{M}^{-1/2}$ is an isometry as stated above. In other words, unit elements are produced by rotating an equilateral element and then mapping it to physical space by $\mathcal{M}^{-1/2}$.

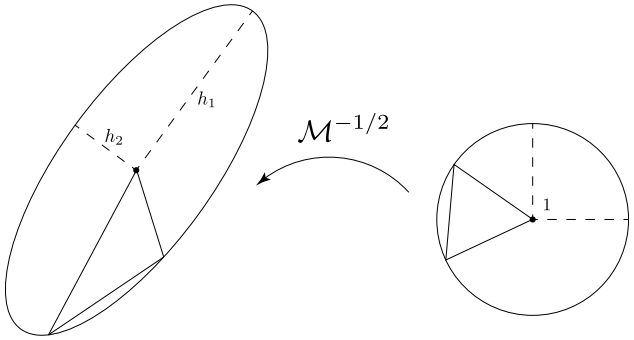

Fig. 1 $\mathcal{M}^{-1/2}$ maps the equilateral element (right) to an element unit in $\mathcal{M}$ (left).

Metric fields and unit meshes Metric fields are (smooth enough) fields of metrics. Geometric quantities such as length are extended by integration, e.g. for $\gamma : [0, 1] \to \mathbb{R}^n$ a curve parameterization,

$$\ell_{\mathcal{M}}(\gamma) = \int_0^1 \left(\gamma'(t)^T \mathcal{M}(\gamma(t))\gamma'(t)\right)^{1/2} dt \tag{3}$$

is the length of the curve $\gamma([0, 1])$ in the metric field $\mathcal{M}(\cdot)$.

A mesh is said to be unit in a metric field $\mathcal{M}$ if all elements are unit for $\mathcal{M}$. This is now defined as either i) having integrated length one edges or ii) each element being unit in the metric field collocated at a point within it. These definitions are not equivalent, but they are consistent with each other as $h \to 0$. As such, there is some flexibility in how these definitions are used. For instance, edge-based remeshing primitives [33–36] make use of the edge-length-based definition, whereas quality-based smoothing [37, 38] may collocate the metric field at element barycentres. Neither is more legitimate than the other, as unit meshes cannot strictly be produced, if only because metric fields are arbitrary whereas meshes are limited to particular element types (linear, quadratic, etc) and offer, at best, a piecewise polynomial approximation of $\mathcal{M}^{-1/2}$.

Assuming a mesh $\mathcal{H}$ is unit in a metric field $\mathcal{M}$, error estimates can be derived over $\mathcal{H}$ as a function of $\mathcal{M}$ only. As such, the design space for error minimization is no longer encumbered with the discrete nature of the variable (here meshes), rather it consists only in smooth functions (metric fields). A canonical example is interpolation error over linear meshes. Denoting $e_{\mathcal{H}} f$ the Lagrange P^1 interpolation error over $\mathcal{H}$ of a function f, and assuming f is quadratic of Hessian H_f, then [2]

$$\|e_{\mathcal{H}} f\|^p_{L^p(\mathcal{H})} \leq C \int \det \mathcal{M}^{-1/2} \left|\mathrm{tr}\left(\mathcal{M}^{-1/2}(x)|H_f(x)|\mathcal{M}^{-1/2}(x)\right)\right|^p dx \tag{4}$$

where C is a numeric constant depending only on the space dimension. This inequality is reached for $p = 1$ and if H is positive definite. The right-hand side can be minimized for $\mathcal{M}$ via calculus of variation, providing optimal metric fields (thus unit meshes) to control a priori the L^p interpolation error of f. This is for instance the case in [9, 39, 40], but more general errors such as on quantities of interest in aeronautics can be minimized [1, 41, 42]

Similar methods can be derived for a posteriori control of generic errors. MOESS [3–6] stages local mesh modifications followed by fast local resolves, thus associating metric changes to observed errors changes. These metric-error change pairs are then used to regress a generic error model. Finally, this generic error model is minimized to provide an optimal change in the implied metric field. A major advantage of this approach is the ability to provide metric-based control of any error via numerical evaluation rather than a priori analytical derivation.

Embedded metric fields A metric field family $(\mathcal{M}_h)_{h>0}$ is said to be embedded if there exists some base metric field $\mathcal{M}$ such that $\mathcal{M}_h = h^{-2}\mathcal{M}$. This notion is the analogous in a metric-based context of mesh sizes bounded by Ch. As prescribed element sizes are the eigenvalues of $\mathcal{M}_h^{-1/2} = h\mathcal{M}^{-1/2}$, it is clear that they are a $O(h)$.

B. High-order meshes

This Section introduces the notations used for high-order meshes in this paper. k designates the simplex topological dimension, d a degree and n the space dimension. Unless otherwise stated, $n = k$, and these constants are omitted from notations. K designates a k-simplex of degree d. The barycentric domain is defined by $\widehat{K} = \{\xi \in [0,1]^{k+1},\ \sum \xi_i = 1\}$. Similarly, let $\widehat{K}_k^d = \{\alpha \in [\![0,d]\!]^{k+1}, \sum \alpha_i = d\}$ be the set of multi-indices for homogeneous degree d $(k+1)$-variate polynomials. The Bernstein polynomial of index α is defined as

$$\forall \xi \in \widehat{K},\ B_\alpha(\xi) = \frac{d!}{\alpha_1!...\alpha_{k+1}!}\xi_1^{\alpha_1}...\xi_{k+1}^{\alpha_{k+1}} \tag{5}$$

The Bernstein polynomials $(B_\alpha)_{\alpha\in\widehat{K}_k^d}$ form a basis of $(k+1)$-variate homogeneous degree d polynomials. The Lagrange polynomial of index α, ϕ_α, is defined by

$$\forall \beta \in \widehat{K}_k^d,\ \phi_\alpha(\beta/d) = \delta_{\alpha\beta} \tag{6}$$

where $\delta_{\alpha\beta} = 1$ if $\alpha = \beta$ and 0 otherwise. This corresponds to regularly spaced Lagrange nodes. The Lagrange polynomials also span a basis of $(k+1)$-variate homogeneous degree d polynomials. When the multi-indices are written *in extenso* they are not written as tuples but rather as e.g. 210. Thus we may write the Bernstein function B_{2101} or the Lagrange function L_{2000}.

A high-order element K is defined by a homogeneous polynomial F_K over the barycentric domain. Its coefficients in the Bernstein basis are called Bézier control points and, in the Lagrange basis, Lagrange nodes. The former are denoted P_α and the latter L_α. Thus

$$F_K = \sum P_\alpha B_\alpha = \sum L_\alpha \phi_\alpha. \tag{7}$$

The Lagrange nodes all lie on the image by F_K of $\widehat{K}$ (the element proper). Only the control points of index de_i (such as $P_{de_1} = P_{d000}$) lie on the element; these are its vertices.

Bézier offsets Lastly, let us introduce a rewrite of the mapping in terms of Bézier control point offsets to the straight control points. Let us denote the offsets as $\Delta_\alpha = P_\alpha - \frac{\alpha_i}{d}P_{de_i}$. For instance, $\Delta_{110} = P_{110} - \frac{1}{2}(P_{200} + P_{020})$ or $\Delta_{121} = P_{121} - \frac{1}{4}(P_{200} + 2P_{020} + P_{002})$. Then [26]:

$$F_K(\xi) = \sum_{i=1}^{k+1} \xi_i P_{de_i} + \sum_{\alpha\in\widehat{K}_k^d} \Delta_\alpha B_\alpha(\xi). \tag{8}$$

The P_{de_i} are the vertices of K, and the offsets at vertices (for some $\alpha = de_j$) vanish. Thus the sum written, for convenience, over all possible indices, only concerns non-vertex control points (or rather their offsets). Let us illustrate in the quadratic case. The vertex indices are 200, 020, 002 and the edge indices are 011, 101 and 110. The offsets at the vertices Δ_{200}, Δ_{020} and Δ_{002} vanish. Thus any quadratic triangle mapping can be written as

$$F_K(\xi) = \xi_1 P_{200} + \xi_2 P_{020} + \xi_3 P_{002} + 2\xi_1\xi_2\Delta_{110} + 2\xi_2\xi_3\Delta_{011} + 2\xi_3\xi_1\Delta_{101}. \tag{9}$$

Notice that the factors against vertices are linear regardless of element degree. Thus element non-linearity is entirely governed by these offsets between control points and the regularly-spaced nodes (such as $\frac{1}{2}(P_{200} + P_{020})$).

k-variate mapping Note all previously defined functions (the bases and element mapping) are $(k+1)$-variate. The reference k-simplex is typically defined as $\widetilde{K} = \{x \in [0,1]^k,\ \sum x_i \le 1\}$. A bijection between the reference element $\widetilde{K}$ and the barycentric domain $\widehat{K}$ is usually chosen as $\phi : \xi \in \widehat{K} \mapsto (\xi_2, ..., \xi_{k+1}) \in \widetilde{K}$, corresponding to the reference element with vertices $P_1 = 0$, $P_2 = e_1$ through $P_{k+1} = e_k$ with e_i the canonical basis vectors of $\mathbb{R}^k$. The inverse of this function is given by $\phi^{-1}(x) = (1 - x_1 - ... - x_k, x_1, ..., x_k)$.

We refer to the k-variate polynomials as the above (Bernstein, Lagrange, element mapping) composed with this choice of ϕ^{-1}. It follows that, if $\widetilde{F}_K$ is the k-variate element mapping, then $\partial_i\widetilde{F}_K = (\partial_{i+1} - \partial_1)F_K$. Its Jacobian matrix is then

$$\partial\widetilde{F}_K = \begin{pmatrix} (\partial_2 - \partial_1)F_K^T \\ ... \\ (\partial_{k+1} - \partial_1)F_K^T \end{pmatrix}. \tag{10}$$

We abusively conflate $\widetilde{F}_K$ and F_K depending on context; in particular, the Jacobian matrix of F_K refers to that of $\widetilde{F}_K$, as for all other derivatives.

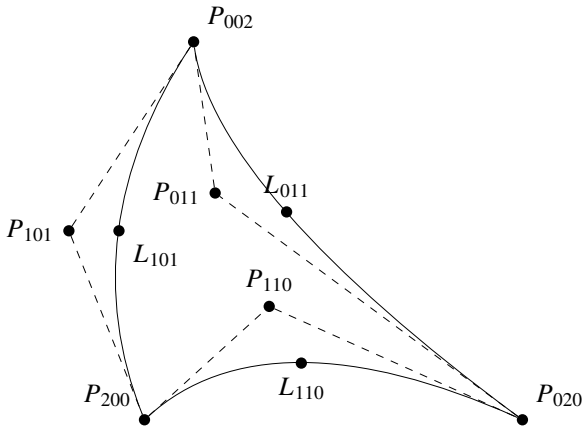

(a) P^2 Bézier triangle: control points $(P_\alpha)_\alpha$ and Lagrange nodes $(L_\alpha)_\alpha$. Control net in dashed lines.

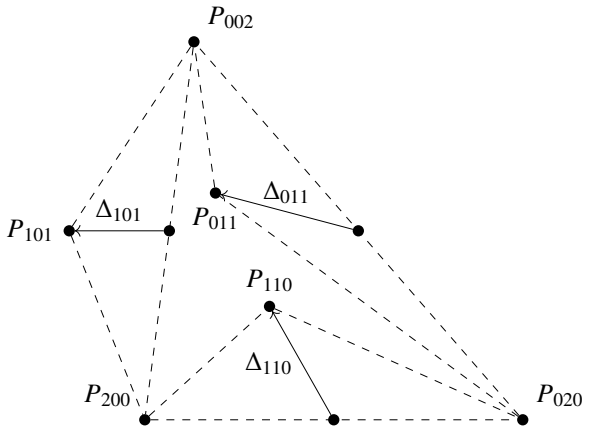

(b) P^2 Bézier triangle: offsets $(\Delta_\alpha)_\alpha$. Control net and subjacent linear element in dashed lines.

III. High-order unit elements

Metric-based adaptation is enabled by defining a so-called unit relationship between metric fields and meshes. The main idea is that all element-dependent quantities can be expressed in terms of the metric field.

This definition must respect some properties. From a practical standpoint, a metric or metric field should not define a unique element, but a class of unit elements. In the linear case, these are all similar up to a rotation. This freedom is necessary to ensure metric-based meshing remains feasible.

At the same time, for error estimation, the fact an element is unit in a given metric field must provide enough information to construct tight error bounds. Thus the equivalence class of unit elements should not be too large. Ideally, mapping derivatives should be explicitly given by the metric field, in order to translate quantities arising in error estimation in metric terms. These metric terms should ideally be invariant over the equivalence class of unit elements, rather than need to be brutally bounded. The opposite of this is a criterion like $\|D^2 F_K\| \leq Ch^2$. From this, it is possible to give interpolation error bounds [19], but all information of how curvature affects the error has been lost.

Finally, constructing unit curved meshes must remain computationally cheap, as the expected benefit of curvature adaptation is to accelerate the computational pipeline. As such, we seek to avoid any variational or optimization statements. Instead, we will find simple geometric criteria to construct unit curved elements in one step from a unit linear element.

In this Section, we detail the generalization of the unit definition to high-order elements. The minimal object in which a linear element may be unit is the single metric. We will illustrate that the analogous notion for quadratic elements is unitness in a metric field of affine square root inverse ($\mathcal{M}^{-1/2}$). Using this minimal definition, we provide exact criteria of high-order unitness. The first criterion concerns the Jacobian of the element mapping collocated, say, at the element barycenter. The second criterion concerns the second derivatives of the element mapping, which it relates to first derivatives of $\mathcal{M}^{-1/2}$. Strictly speaking, these form a fixed-point problem. But using asymptotic estimates in the case of embedded metric fields $h^{-2}\mathcal{M}$, it is possible to show the first step of curving from a linear element yields an element that respects the unit relationships up to a negligible term of h. Similar reasoning allows to relax the definitions to arbitrary smooth metric fields. It is also possible to show meshes unit in an embedded metric field are regular in the sense of [32], thus optimal interpolation error rate $p + 1$ is obtained regardless of the base metric $\mathcal{M}$.

Practical derivations for P^2 triangles and tetrahedra are given in Section IV.

A. General definition of high-order unit elements

1. Reformulation of linear unitness

We start by rewriting the unit mesh definition for linear meshes in a manner that will be appropriate to generalize to high-order meshes. An edge-length-based definition does not prove sufficient for high-order elements. Instead, the traditional definition for linear meshes is written in terms of the element mapping F_K.

Alternate definition using the element mapping In this section, the k-variate element mapping is considered. The Jacobian matrix is thus $(\partial_2 - \partial_1 \ \ldots \ \partial_{k+1} - \partial_1)$ of the $(k+1)$-variate mapping. We still denote ξ for the (k-variate $(\xi_2, \ldots \xi_{k+1})$) variable by abuse of notations.

A linear element K being unit in a metric $\mathcal{M}$ is equivalent to there existing a regular element K_0 and rotation matrix R such that $K = \mathcal{M}^{-1/2} R K_0$. This can be restated in terms of the element mapping F_K of K and F_0 of K_0:

$$F_K = \mathcal{M}^{-1/2} R F_0 \tag{11}$$

Translation-invariant expressions would be preferable. Let $\xi_0 \in \widehat{K}$ be a barycentric coordinate of reference. Then, for all ξ, $F_K(\xi) - F_K(\xi_0) = \mathcal{M}^{-1/2} R(F_0(\xi) - F_0(\xi_0))$. The regular element F_0 is linear, thus of mapping $F_0(\xi) = F_0(\xi_0) + \partial F_0^T(\xi_0)(\xi - \xi_0)$. It follows that K is unit in $\mathcal{M}$ iff, for all ξ_0 and ξ,

$$F_K(\xi) - F_K(\xi_0) = \mathcal{M}^{-1/2} R \partial F_0^T (\xi - \xi_0) \tag{12}$$

This can be interepreted as follows. ξ_0 is a point of reference and $\xi - \xi_0$ a displacement in $\widehat{K}$. A displacement within K is mapped from a displacement within RK_0 by $\mathcal{M}^{-1/2}$.

Linear unit element K_0 will always be a linear element so there is no loss of generality to simplify $F_0(\xi) - F_0(\xi_0)$ into $\partial F_0^T(\xi - \xi_0)$. However, linearity of F_K has not been used at all (save for to consider the above means K is unit) thus treating F_K as an affine function at this stage would induce loss of generality. Nonetheless, if F_K is linear, then

$$\partial F_K^T(\xi - \xi_0) = \mathcal{M}^{-1/2} R \partial F_0^T (\xi - \xi_0) \tag{13}$$

for all ξ. Then, by identification of the polynomial's coefficients,

$$\partial F_K^T = \mathcal{M}^{-1/2} R \partial F_0^T \tag{14}$$

This relationship is not particularly new, and has already been used to derive error estimators on linear meshes either a priori [2] or a posteriori with MOESS [3–6]. However, it is helpful to derive it from "first principles" in order to carefully generalize this concept to high-order meshes.

2. Extensions to high-order meshes

Equation (14) is straightforward to generalize to high-order meshes. If K is a degree d element, its Jacobian matrix is degree $d-1$, and the right-hand side (excluding $\mathcal{M}^{-1/2}$) is constant, thus $\mathcal{M}^{-1/2}$ should, formally, be some degree $d-1$ polynomial. Moreover, $\mathcal{M}$ should be a function of the computational domain Ω rather than the element K. We arrive at: there exists a rotation R, s.t. for all $\xi \in \widehat{K}$, $\partial F_K(\xi) = \mathcal{M}^{-1/2}(F_K(\xi)) R \partial F_0^T$ where $\mathcal{M}^{-1/2} \circ F_K$ is degree $d-1$ polynomial.

One issue arises. When differentiating the relationship, Eq. (14), the left-hand side becomes a 3-tensor with a certain symmetry. This symmetry is not present in the right-hand side unless a constraint is placed on the metric field:

$$\forall (i,j,k), \ \sum_t \mathcal{M}_{ti}^{-1/2} \partial_t \mathcal{M}_{kj}^{-1/2} - \mathcal{M}_{tj}^{-1/2} \partial_t \mathcal{M}_{ki}^{-1/2} = 0 \tag{15}$$

Details for deriving this constraint are in Appendix A. We can attempt to interpret this condition as follows; assume that, at some $x \in \Omega$, that $G_x : y \mapsto \mathcal{M}^{-1/2}(x) y$, and differentiate $\mathcal{M}^{-1/2} \circ G_x$:

$$\partial_i \mathcal{M}_{jk}^{-1/2} \circ G_x = \sum_t \partial_i G_x^{(t)} \partial_t \mathcal{M}_{jk}^{-1/2} = \sum_t \mathcal{M}_{ti}^{-1/2} \partial_t \mathcal{M}_{jk}^{-1/2} \tag{16}$$

Thus Eq. (15) at x is equivalent to

$$\forall (i,j,k), \ \partial_i \mathcal{M}_{jk}^{-1/2} \circ G_x = \partial_k \mathcal{M}_{ji}^{-1/2} \circ G_x. \tag{17}$$

Since $\mathcal{M}^{-1/2}$ is symmetric, all indices i, j, k commute. In other words, the derivatives 3-tensor of $\mathcal{M}^{-1/2} \circ G_x$ at x is symmetric.

Definition III.1 (Unit Jacobian)**.** Let K be a k-simplex and $\mathcal{M}$ a metric field such that $\mathcal{M}^{-1/2} \circ F_K$ is a degree $d-1$ polynomial. Moreover $\mathcal{M}^{-1/2}$ satisfies the condition:

$$\forall (i,j,k),\ \sum_t \mathcal{M}_{ti}^{-1/2} \partial_t \mathcal{M}_{kj}^{-1/2} - \mathcal{M}_{tj}^{-1/2} \partial_t \mathcal{M}_{ki}^{-1/2} = 0. \tag{18}$$

Then, K is unit in $\mathcal{M}$ if there exists a rotation matrix R such that, for all $\xi \in \widehat{K}$,

$$\partial F_K(\xi) = \mathcal{M}^{-1/2}(F_K(\xi)) R \partial F_0^T. \tag{19}$$

This definition is well-posed as the compatibility condition enforcing $\partial_{ij} F_K = \partial_{ji} F_K$ is not contradicted, and we will show an element is uniquely defined from Eq. (19). Unicity is important for practical purposes but, for the purpose of the definition being well formed, it suffices that such an element may exist.

A similar definition is obtained by reverting to the more general relationship in Eq. (12), which does not assume linearity of F_K. Similarly, Eq. (12) cannot be satisfied if $\mathcal{M}^{-1/2} \circ F_K$ is not degree $d-1$ polynomial.

Definition III.2. Let K be a k-simplex and $\mathcal{M}$ a metric field such that $\mathcal{M}^{-1/2} \circ F_K$ is a degree $d-1$ polynomial. K is unit in $\mathcal{M}$ at $\xi_0 \in \widehat{K}$ if there exists a rotation matrix R such that, for all $\xi \in \widehat{K}$,

$$F_K(\xi) - F_K(\xi_0) = \mathcal{M}^{-1/2}(F_K(\xi)) R \partial F_0^T (\xi - \xi_0). \tag{20}$$

Let us compare, briefly, the two definitions. Def. III.1 relates the Jacobian matrix of K to that of K_0 through the metric field, whereas Def. III.2 relates displacements about a barycentric coordinate ξ_0 in K to displacements in K_0 through the metric field. Def. III.1 requires a constraint on the metric field, which Def. III.2 does not at first glance. However, we will show that defining the mesh-intrinsic metric field using Def. III.2 requires the same constraint. The constraint is, however, not required to construct K from $\mathcal{M}$ using Def. III.2, whereas it must be taken into account explicitly if Def. III.1 is used. Def. III.2 introduces a "reference" barycentric coordinate ξ_0, and may thus appear restrictive. However, we will show that, if K is unit in an embedded metric $\mathcal{M}_h$ at some ξ_0, then it is unit in any other ξ_1 up to negligible terms of h.

In summary, the definitions are consistent asymptotically (when embedded metric fields are considered). Def. III.2 is easier to manipulate as symmetry of the mapping Hessian is found in metric-bound expressions with no additional effort. Furthermore, the constraint on the metric does not appear explicitly in Def. III.2, but needs to be introduced to ensure a metric field can be constructed from K. Def. III.1 is undoubtedly more elegant, but care is required to take into account the metric compatibility relationship when differentiating it. It does not need any asymptotic arguments to provide a relationship analogous to the linear case (no ξ_0), and the constraint on the element Jacobian is familiar, as it is the same expected of a linear element unit in a metric.

As appealing as Def. III.1 may be, the analysis here proceeds using Def. III.2, as this is the one obtained with the fewest assumptions on F_K. We will also show that Def. III.1 is obtained as a consequence of Def. III.2. We demonstrate this for the case of quadratic simplices, and provide simple relationships to explicitly construct unit elements.

B. Geometric relationships for unit P^2 simplices

We now consider P^2 simplices and seek to express their mapping derivatives at ξ_0 as a function of the metric. This will, ultimately, provide formulas for unit control point placement, and for error estimation.

Notations If $F : \mathbb{R}^n \to \mathbb{R}^n$ is a vector-valued function, we denote ∂F as its Jacobian matrix defined by $(\partial F)_{ij} = \partial_i F_j$. Note, if J is a matrix and $G : x \mapsto Jx$, then $\partial G = J^T$. This convention is used for consistency with cache-effective storage in C array convention. If $M : \mathbb{R}^n \to \mathcal{M}_n$ is a $n \times n$ matrix-valued function, we denote ∂M its "Jacobian" 3-tensor defined by

$$(\partial M)_{ijk} = \partial_i F_{jk}. \tag{21}$$

With these notations, the vector-valued F Hessian, $\partial^2 F = \partial(\partial F)$, has general term $(\partial^2 F)_{ijk} = \partial_{ij} F_k$. We define the following products between a 3-tensor T and matrix A yielding a 3-tensor:

$$(T \times_1 A)_{ijk} = \sum_s T_{sjk} A_{si}, \quad (T \times_2 A)_{ijk} = \sum_s T_{isk} A_{sj}, \quad (T \times_3 A)_{ijk} = \sum_s T_{ijs} A_{sk}. \tag{22}$$

The left products are defined by $T \times_i A = A^T \times_i T$. Products are similarly defined if A is a vector, yielding a matrix, e.g. $(T \times_1 A)_{ij} = \sum_s T_{sij} A_s$.

Deriving geometric relationships The affine metric field is expanded as

$$\mathcal{M}_{ij}^{-1/2}(F_K(\xi)) = \mathcal{M}_{ij}^{-1/2}(F_K(\xi_0)) + T(\xi_0) \times_1 (\xi - \xi_0) \tag{23}$$

with $T = \partial \mathcal{M}^{-1/2} \circ F_K = \partial F_K \times_1 \partial \mathcal{M}^{-1/2}(F_K)$. A similar expansion of F_K writes:

$$F_K(\xi) - F_K(\xi_0) = \partial F_K^T(\xi_0)(\xi - \xi_0) + \frac{1}{2} \sum_{st} (\xi - \xi_0)_s (\xi - \xi_0)_t \partial_{st} F_K(\xi_0) \tag{24}$$

Using both expansions in Eq. (20) gives

$$\partial F_K^T(\xi_0)(\xi - \xi_0) + \frac{1}{2} \sum_{st} (\xi - \xi_0)_s (\xi - \xi_0)_t \partial_{st} F_K(\xi_0) = \left[\mathcal{M}^{-1/2}(F_K(\xi_0)) + T \times_1 (\xi - \xi_0) \right] R \partial F_0^T(\xi - \xi_0). \tag{25}$$

Here, ξ is the "reduced" barycentric coordinates (ξ_2 through ξ_{k+1}), thus of all independent components. It follows that the terms are of their apparent degree. On the left-hand side, we have a purely P^1 term summed to a purely P^2 term, and similarly on the right-hand side. Thus, for all ξ,

$$\begin{aligned} \partial F_K^T(\xi_0)(\xi - \xi_0) &= \mathcal{M}^{-1/2} R \partial F_0^T(\xi - \xi_0) \\ \text{and} \quad \frac{1}{2} \sum_{st} (\xi - \xi_0)_s (\xi - \xi_0)_t \partial_{st} F_K(\xi_0) &= \left[T \times_1 (\xi - \xi_0) \right] R \partial F_0^T(\xi - \xi_0). \end{aligned} \tag{26}$$

Geometric equations These derivations are provided in Appendix B with the results presented here. Let $N = R \partial F_0^T$ and

$$T^{\mathcal{M}}(\xi_0) = \mathcal{M}^{-1/2}(F_K(\xi_0)) \times_1 \partial \mathcal{M}^{-1/2}(F_K(\xi_0)) \tag{27}$$

If K is unit in $\mathcal{M}$ at ξ_0, then:

- we have a first-order geometric relationship already present in the linear mesh case:

$$\partial F_K(\xi_0) = N^T \mathcal{M}^{-1/2}(F_K(\xi_0)) \tag{28}$$

- and now also a second-order geometric relationship:

$$\partial_{ij}^2 F_K^{(k)} = \sum_{st} (N_{sj} N_{ti} + N_{si} N_{tj}) T_{skt}^{\mathcal{M}}(\xi_0) \tag{29}$$

If the metric field is constant, the second equation enforces vanishing second derivatives of the element, and the first condition is the same as in the classic linear unit mesh framework. Thus this is consistent with the classic framework [2].

Continuous mesh The geometric relationships in Eqs. (28) and (29) concern a collocation point ξ_0 and a particular type of metric field ($\mathcal{M}^{-1/2}$ linear). We can relax these as follows. Let $(\mathcal{M}_h)_{h>0}$ be an embedded family of metric fields, i.e. $\mathcal{M}_h^{-1/2} = h \mathcal{M}^{-1/2}$. If K is unit in $\mathcal{M}_h$ at any ξ_0 then

$$\forall \xi \in \widehat{K},\ \partial F_K(\xi) = \partial F_0 R^T \mathcal{M}_h^{-1/2}(F_K(\xi)) + O(h^2). \tag{30}$$

and, if $\mathcal{M}$ follows the condition (15), then

$$\forall \xi \in \widehat{K},\ \partial_{ij}^2 F_K^{(k)} = \sum_{st} (N_{sj} N_{ti} + N_{si} N_{tj}) T_{skt}^{\mathcal{M}_h}(\xi) + O(h^3) \tag{31}$$

and all explicit quantities in Eq. (30) are $O(h)$, and $O(h^2)$ in Eq. (31). These are formal equations that can, in practice, be collocated at any point (say edge middle or element center), or integrated, or substitute some quantity everywhere (rather than only ξ_0) in error estimation, thus offering more flexibility than requiring a specific fixed ξ_0. Essentially they offer the knowledge that any ξ_0 can be chosen and the equations remain consistent as h goes to 0. Equivalently, this is to say Def. III.2 is consistent with the more desirable Def. III.1, which is the most straightforward generalization of the classic linear framework, at the cost of a condition on the metric field. Note that this condition will become necessary, if not to preserve symmetry of the right-hand side of (31), then to ensure uniqueness of the metric field associated to a given element.

C. Properties

In this Subsection, we show some asymptotic behaviour of F_K if K is unit in an embedded metric field $\mathcal{M}_h$. Notably, unit elements become straighter as mesh sizes go to 0, independently of the base metric. This guarantees interpolation error converges at optimal rate $p+1$ [19] rather than $\lfloor p/q \rfloor + 1$ [22, 23], q the geometric degree. We also show a unique mesh-intrinsic metric exists (that is, compute $\mathcal{M}$ from K). This is important for mesh adaptation, as otherwise an optimization statement with $\mathcal{M}$ as the design variable risks ill-posedness. Finally, that all variants of the unit definition are consistent, that is deviate up to negligible terms of h.

Mapping from the ideal element Mapping from the ideal rather than reference element exposes the rotation matrix so that it may simplify more readily in derivations. An example is given when generalizing the multi-scale estimator to curved meshes in Section V. Going back to the very start, introduce $x = F_{K_0}(\xi)$, then the first principle writes

$$F_{K_0 \to K}(x) - F_{K_0 \to K}(x_0) = \mathcal{M}^{-1/2} R x \tag{32}$$

Now the analysis is the same starting from Eq. (23) replacing F_K with $F_{K_0 \to K}$ and $N = R \partial F_0^T$ with simply R. In the end:

$$\begin{aligned} \partial F_{K_0 \to K}^T &= \mathcal{M}^{-1/2} R \\ \partial_{ij}^2 F_{K_0 \to K}^{(k)} &= \sum_{st} (R_{sj} R_{ti} + R_{si} R_{tj}) T_{skt}^{\mathcal{M}} \end{aligned} \tag{33}$$

with $T^{\mathcal{M}}$ the same tensor as before.

Mesh-intrinsic metric Given an element K, there must exist a unique metric $\mathcal{M}$ in which K is unit. If K is unit in a metric field $\mathcal{M}$ such that $\mathcal{M}^{-1/2} \circ F_K$ is affine, then Eq. (28) provides $\mathcal{M}^{-1/2}(F_K(\xi_0))$. For this refer to e.g. [7], as it is the same classic relationship for linear meshes. Knowing $\mathcal{M}^{-1/2}(F_K(\xi_0))$, we can obtain R and then $\partial \mathcal{M}^{-1/2} \circ F_K(\xi_0)$ using Eq. (29). The rotation is uniquely defined from the linear relationship, we detail this computation in Section IV.B. Thus for all i, j, s, t, $N_{sj} N_{ti} + N_{si} N_{tj}$ is known. Then

$$\partial_{ij}^2 F_K^{(k)} = \sum_{st} (N_{sj} N_{ti} + N_{si} N_{tj}) \sum_u \mathcal{M}_{us}^{-1/2} \partial_u \mathcal{M}_{kt}^{-1/2} \tag{34}$$

Let us set k. The unknowns are the partial derivatives of $\mathcal{M}^{-1/2}$. This is a set of $|\{i \leq j\}|$ linear relationships. It follows unicity can only be guaranteed if there are as many unknowns, here the $X_{st}^{(k)} = \sum_u \mathcal{M}_{us}^{-1/2} \partial_u \mathcal{M}_{kt}^{-1/2}$ for all s, t. Thus we require the symmetry

$$\sum_u (\mathcal{M}_{ui}^{-1/2} \partial_u \mathcal{M}_{kj}^{-1/2} - \mathcal{M}_{uj}^{-1/2} \partial_u \mathcal{M}_{ki}^{-1/2}) = 0 \tag{35}$$

and this is again the metric compatibility condition Eq. (15), that we now assume is satisfied. Then

$$\partial_{ij}^2 F_K^{(k)} = \sum_{st} (N_{sj} N_{ti} + N_{si} N_{tj}) X_{st}^{(k)} = \sum_{s \leq t} C_{ijst} X_{st}^{(k)} \tag{36}$$

with $C_{ijss} = 2 N_{sj} N_{si}$ and $C_{ijst} = 2(N_{sj} N_{ti} + N_{si} N_{tj})$ if $s \neq t$. Introduce an ordering I e.g., in two dimensions, $I(1,1) = 1$, $I(1,2) = 2$, $I(2,2) = 3$. Then the above writes

$$U^{(k)} = M X^{(k)} \tag{37}$$

where $U^{(k)}$ is a vector of general term $U_{I(i,j)}^{(k)} = \partial_{ij}^2 F_K^{(k)}$, and M is a matrix of general term $M_{I(i,j),I(s,t)} = C_{ijst}$. The matrix is shown to be invertible in the 2D case. We also consider the element mapping from K_0 rather than $\widehat{K}$, such that $N = R$. The rotation matrix writes, for some θ,

$$R = \begin{pmatrix} \cos(\theta) & -\sin(\theta) \\ \sin(\theta) & \cos(\theta) \end{pmatrix}. \tag{38}$$

The C_{ijst} are thus:

$$\begin{aligned}
&C_{1111} = 2\cos(\theta)^2, && C_{1211} = -2\cos(\theta)\sin(\theta), && C_{2211} = 2\sin(\theta)^2\\
&C_{1112} = 4\cos(\theta)\sin(\theta), && C_{1212} = 2(\cos(\theta)^2 - \sin(\theta)^2), && C_{2212} = -4\cos(\theta)\sin(\theta)\\
&C_{1122} = 2\sin(\theta)^2, && C_{1222} = 2\cos(\theta)\sin(\theta), && C_{2222} = 2\cos(\theta)^2
\end{aligned} \tag{39}$$

The matrix is then:

$$M = \begin{pmatrix} C_{1111} & C_{1112} & C_{1122} \\ C_{1211} & C_{1212} & C_{1222} \\ C_{2211} & C_{2212} & C_{2222} \end{pmatrix} = \begin{pmatrix} 2\cos(\theta)^2 & 4\cos(\theta)\sin(\theta) & 2\sin(\theta)^2 \\ -2\cos(\theta)\sin(\theta) & 2(\cos(\theta)^2 - \sin(\theta)^2) & 2\cos(\theta)\sin(\theta) \\ 2\sin(\theta)^2 & -4\cos(\theta)\sin(\theta) & 2\cos(\theta)^2 \end{pmatrix} \tag{40}$$

where its determinant simplifies to:

$$\det M = 8\cos(\theta)^6 + 24\cos(\theta)^4\sin(\theta)^2 + 24\cos(\theta)^2\sin(\theta)^4 + 8\sin(\theta)^6 = 8(\cos(\theta)^2 + \sin(\theta)^2)^3 = 8. \tag{41}$$

It follows that the system is invertible for all k, thus that the $\sum_u \mathcal{M}_{ui}^{-1/2}(F_K(\xi_0))\partial_u \mathcal{M}_{kj}^{-1/2}(F_K(\xi_0))$ are uniquely determined from the second derivatives of F_K, for all i, j, k. We assume this matrix is also invertible in 3D. To finish, we obtain the derivatives of $\mathcal{M}$ using the $X^{(k)}$. Notice

$$\sum_u \mathcal{M}_{ui}^{-1/2}(F_K(\xi_0))\partial_u \mathcal{M}_{kj}^{-1/2}(F_K(\xi_0)) \iff X^{jk} = \mathcal{M}^{-1/2}\nabla\mathcal{M}_{jk}^{-1/2} \tag{42}$$

with X^{jk} the vector of term $X_i^{jk} = X_{ij}^{(k)}$. The systems can be solved independently for each $\nabla\mathcal{M}_{jk}^{-1/2}$.

In the particular case where K is linear, the $X^{(k)}$ vanish, thus the $\nabla\mathcal{M}_{jk}^{-1/2}$ vanish as well. In this case, we obtain the same mesh-intrinsic metric as in the linear case. As noticed previously, K is linear if the metric field is constant. Thus an element K is linear if, and only if, the metric field is constant over K. Furthermore, if K is linear, its intrinsic metric is the same as in the classic framework.

Asymptotic curvature In what follows, we consider an embedded family of metric fields $(\mathcal{M}_h)_{h>0}$ verifying $\mathcal{M}_h^{-1/2} = h\mathcal{M}^{-1/2}$ for some base metric field $\mathcal{M}$ (indeed, $\mathcal{M}_1$). The parameter h thus scales metric-induced sizes uniformly across the domain. If K is unit in $\mathcal{M}_h$ at ξ_0,

$$\partial F_K(\xi_0) = h\mathcal{M}^{-1/2}(F_K(\xi_0))N \tag{43}$$

and $T^{\mathcal{M}_h} = \mathcal{M}_h^{-1/2}(F_K(\xi_0)) \times_1 \partial\mathcal{M}_h^{-1/2}(F_K(\xi_0)) = h^2 T^{\mathcal{M}}$, thus

$$\partial_{ij}^2 F_K^{(k)} = h^2 \sum_{st}(N_{sj}N_{ti} + N_{si}N_{tj})T_{skt}^{\mathcal{M}} \tag{44}$$

In other words (formally), if F_K is unit in $\mathcal{M}_h$, then

$$\partial F_K = O(h) \quad \text{and} \quad \partial^2 F_K = O(h^2). \tag{45}$$

It follows that unit meshes become straighter at convergence. This also corresponds to the definition of elements in a regular isoparametric finite element family, see e.g. [32] or Thm. 4.3.3 in [43]. Faster convergence of the high-order element mapping components in necessary to preserve interpolation error convergence. From a practical standpoint, unit meshes will also always become valid for h small enough (provided the subjacent linear meshes are valid). This is also shown in [43].

Choice of collocation point Let us show the choice of ξ_0 is inconsequential at convergence. Let ξ_0 and ξ_1 be two barycentric coordinates and K be unit in $\mathcal{M}_h$ at ξ_0. Starting from the second derivatives:

$$\begin{aligned}
T^{\mathcal{M}_h}(\xi_0) = \mathcal{M}_h^{-1/2}(F_K(\xi_0)) \times_1 \partial\mathcal{M}_h^{-1/2}(F_K(\xi_0)) &= \left[\mathcal{M}_h^{-1/2}(F_K(\xi_1)) + \left[\partial\mathcal{M}_h^{-1/2} \circ F_K\right](\xi_1) \times_1 (\xi_1 - \xi_0)\right] \\
&= T^{\mathcal{M}_h}(\xi_1) + O(h^3) \times_1 \partial\mathcal{M}_h^{-1/2}(F_K(\xi_1))
\end{aligned} \tag{46}$$

as $\partial \mathcal{M}_h^{-1/2}$ is constant over K, and $\partial \mathcal{M}_h^{-1/2} \circ F_K$ is a $O(h^2)$. Thus

$$\partial^2_{ij} F^k_K = \sum_{st} (M_{sj} M_{ti} + M_{tj} M_{si}) T^{\mathcal{M}_h}_{skt}(\xi_1) + O(h^3) \tag{47}$$

as the second derivatives are constant over the quadratic element. Similarly,

$$\partial F^T_K(\xi_1) = \mathcal{M}^{-1/2}(F_K(\xi_1))N + O(h^2). \tag{48}$$

These are the unit relations at ξ_1 up to negligible remainders.

Practically speaking, this means Def. III.2 can be applied at any ξ_0 and yield consistent results at convergence. It is common for linear remeshers to consider different metrics depending on circumstances. For instance, quality may be measured using the metric at the barycenter, or by quadrature; edge length involving the metric along the edge may be used, or instead a comparison of the Jacobian matrix with the metric at the barycenter.

Since this is true for all ξ_1, we have also shown the fully continuous Eqs. (30) and (31).

Fixed point problem The unit Eqs. (28) and (29) form a fixed-point problem. Indeed, the mapping F_K is determined from the metric evaluated at $F_K(\xi_0)$. From a practical standpoint, suppose K is straight, and unit per the first relationship on the Jacobian matrix, where the barycenter of the straight element is used to evaluate $\mathcal{M}^{-1/2}$ and $T^{\mathcal{M}}$. The element is curved using a single iteration the fixed point problem below, which results in an element that is unit enough per the rigorous definition.

Denote F_1 the subjacent linear element to F_K and let us assume F_1 is already unit in $\mathcal{M}$, as the result of linear mesh adaptation. The difference $F_K - F_1$ depends only on the second derivatives of F_K, as illustrated with the offsets in Eq. (8). Assume the second derivatives of F_K are set to:

$$\partial_{ij} F^k_K(\xi_0) = \sum_{st} (N_{sj} N_{ti} + N_{si} N_{tj}) T^{\mathcal{M}}_{skt}(F_1(\xi_0)). \tag{49}$$

with N the $R\partial F_0^T$ associated to F_1. The right-hand side is expanded to

$$T^{\mathcal{M}}_{skt}(F_1(\xi_0)) = T^{\mathcal{M}}_{skt}(F_K(\xi_0)) + E_h(||F_1 - F_K||) \tag{50}$$

with $E_h(||F_1 - F_K||) \leq Ch^2||F_1 - F_K||$. C is some constant that does not depend on h. Note that these are physical derivatives, i.e. not of e.g. $\mathcal{M}^{-1/2} \circ F_K$ but of $\mathcal{M}^{-1/2}$ proper, and so $\partial T^{\mathcal{M}}_{skt} = O(h^2)$. The second derivatives of F_K become:

$$\partial_{ij} F^k_K(\xi_0) = \sum_{st} (N_{sj} N_{ti} + N_{si} N_{tj}) T^{\mathcal{M}}_{skt}(F_K(\xi_0)) + E_h(||F_1 - F_K||) \tag{51}$$

Since F_1 is the subjacent linear element of K, they differ only by the offsets $F_K - F_1 = \sum B_\alpha \Delta_\alpha$, thus $\|F_1 - F_K\| \leq C\|\partial^2 F_K\|$. Per Eq. 49, $\|\partial^2 F_K\| \leq Ch^2$. Hence

$$\partial_{ij} F^k_K(\xi_0) = \sum_{st} (N_{sj} N_{ti} + N_{si} N_{tj}) T^{\mathcal{M}}_{skt}(F_K(\xi_0)) + O(h^4) \tag{52}$$

It follows that that the second derivatives are as if computed at the true barycenter, up to a $O(h^4)$ remainder, which is negligible against their own $O(h^2)$ norm. As for the Jacobian matrix,

$$\partial F_K(\xi_0) = \partial F_1(\xi_0) + \partial F_K(\xi_0) - \partial F_1(\xi_0) = \partial F_1(\xi_0) + O(h^2). \tag{53}$$

As the subjacent linear element is unit, $\partial F_1(\xi_0)^T = \mathcal{M}^{-1/2}(F_1(\xi_0))N = \mathcal{M}^{-1/2}(F_K(\xi_0))N + O(h^3)$. Replacing above:

$$\partial F_K(\xi_0) = \mathcal{M}^{-1/2}(F_K(\xi_0))N + O(h^2)$$

In conclusion, although the unit relations form a fixed-point problem, a single iteration of curving from a unit linear element is sufficient to ensure the curved element is unit up to negligible remainders. So, in practice, we can consider this to be a one-step method.

IV. Explicit construction of unit P^2 meshes

In this Section, we detail the application of the unit relationships Eq. (28) and Eq. (29) to triangles and tetrahedra. This separation of unitness between linear and quadratic components of the mapping leads naturally to using degree continuation methods. The linear relationship Eq. (28) is as in linear meshing: the same techniques apply. Thus the subjacent linear mesh is assumed unit. It is then modified exclusively for curvature using Eq. (29).

A. Computing the metric and derivatives

The second order relationship Eq. (29) requires computing the tensor $T^{\mathcal{M}} = \mathcal{M}^{-1/2}(F_K(\xi_0)) \times_1 \partial\mathcal{M}^{-1/2}(F_K(\xi_0))$. If the metric field is given analytically, this is trivial. Otherwise, it is common to interpolate from a background mesh.

Let K' be an element in which $F_K(\xi_0)$ lies. This may be K itself if the metric field is interpolated on K, or it may be a background mesh element. The degree of the element is arbitrary. We consider here degree d' log-Euclidean interpolation over K'. This is defined by

$$\log \mathcal{M}(F_{K'}(\xi)) = \sum_{\alpha \in \widehat{K}_k^{d'}} \phi_\alpha(\xi) \log \mathcal{M}_\alpha \tag{54}$$

where the $\mathcal{M}_\alpha$ are the degrees of freedom (nodal metrics), and the ϕ_α the degree d' Lagrange functions. This interpolation scheme does not yield a linear metric field. However, $\mathcal{M}$ commutes with itself and the identity, thus $\log I - \log \mathcal{M}^{-1/2} - \log \mathcal{M}^{-1/2} = \log \mathcal{M}$ and, since $\log I = 0$,

$$\log \mathcal{M}^{-1/2}(F_{K'}(\xi)) = \sum_{\alpha \in \widehat{K}_k^{d'}} \phi_\alpha(\xi)(-\log \mathcal{M}_\alpha/2) \tag{55}$$

thus the coefficients of $\mathcal{M}^{-1/2}$ are conveniently $-1/2$ those of $\mathcal{M}$ in the Lagrange basis. The metric is typically stored directly in log-format in the background mesh so it is very straightforward to evaluate $\mathcal{M}^{-1/2}$. Physical derivatives are computed using the element Jacobian matrix and the barycentric derivatives, analytically as in [29, 30, 44, 45], or using automatic differentiation [46].

It may prove computationally efficient to first interpolate the metric field coefficients (possibly to the same degree d) at the main element K, and then to interpolate within K. This also leads to a smoother metric within the element, as jumps across background elements are avoided.

The interpolation degree need note relate directly to the fact $\mathcal{M}^{-1/2} \circ F_K$ must be at least linear, as it is the log field which is polynomial here, nor to the degree of K, as presumably other degree basis functions are available. An optimal choice may warrant further investigation.

B. Determining scaling and orientation

Let K be a P^2 element whose subjacent linear element of mapping F_1 verifies Eq. (28). We seek to determine R and, possibly, the scaling λ of the element respective to the metric. The relationship writes

$$\partial F_1(\xi_0) = \lambda \partial F_0 R^T \mathcal{M}^{-1/2} \tag{56}$$

The scaling is obtained by computing the determinant. ∂F_0 is the Jacobian matrix of a regular element. It follows that

$$\partial F_0 \partial F_0^T = \begin{pmatrix} 1 & 1/2 & \cdots \\ 1/2 & \ddots & \ddots \\ \vdots & \ddots & \end{pmatrix} \tag{57}$$

as the i, j-th component is the scalar product between the i-th and j-th edge of K_0, either 1 if $i = j$, or $\cos(\pi/3) = \frac{1}{2}$ otherwise. For $k = 2$, the determinant is $3/4$. For $k = 3$, it is $1/2$. Thus

$$\lambda^k = \begin{cases} 2 \det\left(\mathcal{M}^{1/2}\right) \det\left(\partial F_1(\xi_0)\right) / \sqrt{3} & \text{if } k = 2 \\ \sqrt{2} \det\left(\mathcal{M}^{1/2}\right) \det\left(\partial F_1(\xi_0)\right) & \text{if } k = 3 \end{cases} \tag{58}$$

The rotation matrix is then computed as $R = \partial F_0^{-1} \partial F_1 \mathcal{M}^{1/2} / \lambda$. In what follows, we detail the computations of curvature for triangles and tetrahedra.

C. P^2 triangles

Let K be a P^2 triangle written using the Bézier offsets:

$$\Delta_{011} = P_{011} - \frac{1}{2}(P_{020} + P_{002}), \quad \Delta_{101} = P_{101} - \frac{1}{2}(P_{002} + P_{200}) \quad \text{and} \quad \Delta_{110} = P_{110} - \frac{1}{2}(P_{200} + P_{020}). \tag{59}$$

The mapping is then:

$$F_K(\xi) = \xi_1 P_{200} + \xi_2 P_{020} + \xi_3 P_{002} + 2\xi_2\xi_3\Delta_{011} + 2\xi_3\xi_1\Delta_{101} + 2\xi_1\xi_2\Delta_{110}. \tag{60}$$

Let us compute its second derivatives, omiting the contributions from the main vertices as they will vanish at the second differentiation. Recall the i-th physical (or k-variate) derivative is $\partial_{i+1} - \partial_1$ with ∂_j denoting the barycentric derivatives. The first derivatives are:

$$\begin{aligned} \partial_1 F_K &= 2\xi_3\Delta_{011} - 2\xi_3\Delta_{101} + 2(\xi_1 - \xi_2)\Delta_{110} \\ \partial_2 F_K &= 2\xi_2\Delta_{011} + 2(\xi_1 - \xi_3)\Delta_{101} - 2\xi_2\Delta_{110}, \end{aligned} \tag{61}$$

thus the second:

$$\begin{aligned} \partial_{11} F_K = -4\Delta_{110}, \quad \partial_{22} F_K = -4\Delta_{101} \\ \text{and} \quad \partial_{12} F_K = 2(\Delta_{011} - \Delta_{101} - \Delta_{110}). \end{aligned} \tag{62}$$

Using Eq. (29),

$$\begin{aligned} \Delta_{110}^{(k)} &= -\frac{1}{2}\sum_{st} N_{s1} N_{t1} T_{skt}^{\mathcal{M}} \\ \Delta_{101}^{(k)} &= -\frac{1}{2}\sum_{st} N_{s2} N_{t2} T_{skt}^{\mathcal{M}} \\ \Delta_{011}^{(k)} &= \Delta_{101} + \Delta_{110} + \frac{1}{2}\sum_{st} (N_{s2} N_{t1} + N_{s1} N_{t2}) T_{skt}^{\mathcal{M}} \end{aligned} \tag{63}$$

with $\Delta^{(k)}$ denoting the k-th component of the vector. With these formulas, and the previous computation of R and scaling, it is immediate to curve the element K.

D. P^2 tetrahedra

K is now a P^2 tetrahedron, similarly written using its Bézier offsets:

$$\begin{aligned} F_K(\xi) = \xi_1 P_{2000} + \xi_2 P_{0200} + \xi_3 P_{0020} + \xi_4 P_{0002} \\ + 2\xi_1\xi_2\Delta_{1100} + 2\xi_1\xi_3\Delta_{1010} + 2\xi_1\xi_4\Delta_{1001} + 2\xi_2\xi_3\Delta_{0110} + 2\xi_2\xi_4\Delta_{0101} + 2\xi_3\xi_4\Delta_{0011}. \end{aligned} \tag{64}$$

As previously, we omit contributions from the vertices. The first derivatives are:

$$\begin{aligned} (\partial_2 - \partial_1) F_K(\xi) &= 2(\xi_1 - \xi_2)\Delta_{1100} - 2\xi_3\Delta_{1010} - 2\xi_4\Delta_{1001} + 2\xi_3\Delta_{0110} + 2\xi_4\Delta_{0101} \\ (\partial_3 - \partial_1) F_K(\xi) &= -2\xi_2\Delta_{1100} + 2(\xi_1 - \xi_3)\Delta_{1010} - 2\xi_4\Delta_{1001} + 2\xi_2\Delta_{0110} + 2\xi_4\Delta_{0011} \\ (\partial_4 - \partial_1) F_K(\xi) &= -2\xi_2\Delta_{1100} - 2\xi_3\Delta_{1010} + 2(\xi_1 - \xi_4)\Delta_{1001} + 2\xi_2\Delta_{0101} + 2\xi_3\Delta_{0011} \end{aligned} \tag{65}$$

hence the second:

$$\begin{aligned} (\partial_2 - \partial_1)(\partial_2 - \partial_1) F_K(\xi) &= -4\Delta_{1100} \\ (\partial_3 - \partial_1)(\partial_3 - \partial_1) F_K(\xi) &= -4\Delta_{1010} \\ (\partial_4 - \partial_1)(\partial_4 - \partial_1) F_K(\xi) &= -4\Delta_{1001} \\ (\partial_3 - \partial_1)(\partial_2 - \partial_1) F_K(\xi) &= -2\Delta_{1100} - 2\Delta_{1010} + 2\Delta_{0110} \\ (\partial_4 - \partial_1)(\partial_2 - \partial_1) F_K(\xi) &= -2\Delta_{1100} - 2\Delta_{1001} + 2\Delta_{0101} \\ (\partial_4 - \partial_1)(\partial_3 - \partial_1) F_K(\xi) &= -2\Delta_{1010} - 2\Delta_{1001} + 2\Delta_{0011} \end{aligned} \tag{66}$$

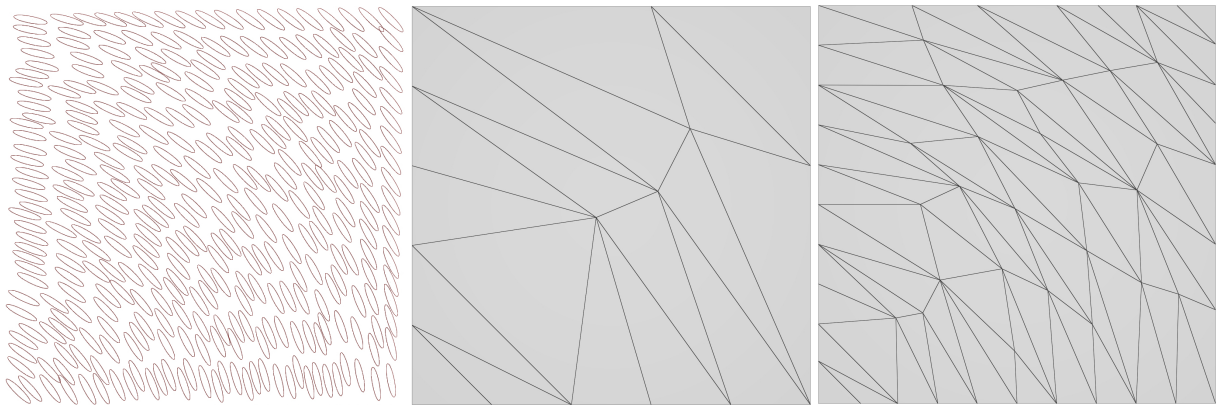

Fig. 3 Left: circular metric field $\mathcal{M}$. Center and right, respectively, coarse and fine linear meshes adapted to $\mathcal{M}$.

The offsets are thus explicitely given by:

$$\begin{aligned}
\Delta_{1100} &= -\frac{1}{2}\sum_{st}(N_{s1}N_{t1})T^{\mathcal{M}}_{skt}(\xi_0), \quad \Delta_{1010} = -\frac{1}{2}\sum_{st}(N_{s2}N_{t2})T^{\mathcal{M}}_{skt}(\xi_0), \quad \Delta_{1001} = -\frac{1}{2}\sum_{st}(N_{s3}N_{t3})T^{\mathcal{M}}_{skt}(\xi_0) \\
\Delta_{0110} &= \Delta_{1100} + \Delta_{1010} + \frac{1}{2}\sum_{st}(N_{s1}N_{t2} + N_{s2}N_{t1})T^{\mathcal{M}}_{skt}(\xi_0) \\
\Delta_{0101} &= \Delta_{1100} + \Delta_{1001} + \frac{1}{2}\sum_{st}(N_{s1}N_{t3} + N_{s3}N_{t1})T^{\mathcal{M}}_{skt}(\xi_0) \\
\Delta_{0011} &= \Delta_{1010} + \Delta_{1001} + \frac{1}{2}\sum_{st}(N_{s2}N_{t3} + N_{s3}N_{t2})T^{\mathcal{M}}_{skt}(\xi_0)
\end{aligned} \tag{67}$$

It suffice to convert the offsets back to control points — e.g. $P_{1100} = \Delta_{1100} + (P_{2000} + P_{0200})/2$ — to obtain the curved element in standard Bézier format.

E. Degree continuation

We propose to first construct a unit linear mesh per the linear relationship (28). This is the classic relationship, any metric-based software can be used for this purpose. A high-order mesh can be treated as linear by first converting control points to offsets. This is straightforward to do if control points are stored separately from vertices, or if they are stored contiguously with an ordering that places all vertices first.

Finally, the offsets are computed as derived above. This is extremely cheap. The most costly computations are to obtain the metric and its derivatives, but these are necessary for any type of current metric-based curving method [29, 30, 44, 45]. This method obtains unit curvature in one step with no need for costly optimization. Strictly speaking, the unit relationships form a fixed-point problem, as the interpolation point is not fixed in physical but in barycentric space, and the element mapping is modified by curving. But we have shown the error after the first fixed-point iteration starting from a linear element is already negligible (in terms of mesh size h).

F. Numerical example

Let us illustrate curvature created by these equations. We consider the metric field

$$\mathcal{M}^{-1/2}(\phi(r,\theta)) = R_\theta \mathrm{diag}(h_1^{-2}, h_2^{-2}) R_\theta^T \tag{68}$$

with $\phi : (r,\theta) \mapsto (r\cos\theta, r\sin\theta)$ the polar coordinates transform, h_1, h_2 two distinct constant sizes, and R_θ the rotation matrix of angle θ. This metric field has axes aligned with the polar coordinate axes and constant sizes. It is illustrated in Fig. 3, together with the meshes we will use, coarse (left) and fine (right). We expect unit meshes in this metric field to follow the main directions of the metric field, i.e. for element edges to approximate circle arcs. Computational details for the derivatives tensor are left in the Appendix C.

A Matlab script implements the offsets computations from the analytical metric and derivatives. Two versions are implemented: using the metric at the element barycenter or at the edge middle. The objective is to show the curvature created by the metric field, the algorithms are extremely simple and summarized in Alg. 1 (per edge) and 2 (per element). In both cases, offsets for each edge are computed once per adjacent element. This is because each element has a distinct rotation matrix and scaling. Note scaling would be 1 for all elements if they were perfectly unit as linear elements, but we must compute it even for an input adapted mesh, to ensure the determinant of the rotation matrix is indeed exactly 1. The offsets are computed by the getoffsetijk (edge) and getoffsets (element). Offset computations are summarized in Alg. 3 and Alg. 4. The scaling and rotation are computed per Sec. IV.B. The metric tensor is computed per Eqs. (63).

Algorithm 1 Edge-based curving

for iface $\leftarrow 1$, nface **do**
  Δ^*_{011} += getoffset011(P_{200}, ..., Δ_{011}, ...)/2
  Δ^*_{101} += getoffset101(P_{200}, ..., Δ_{101}, ...)/2
  Δ^*_{110} += getoffset110(P_{200}, ..., Δ_{110}, ...)/2
end for
for iface $\leftarrow 1$, nface **do**
  [P_{011},P_{011},P_{011}] $\leftarrow$ getpts(P_{200}, ..., Δ^*_{011}, ...)
end for

Algorithm 2 Element-based curving

for iface $\leftarrow 1$, nface **do**
  $[\Delta^*_{011}, \Delta^*_{011}, \Delta^*_{011}]$ += getoffsets(P_{200}, ..., Δ_{011}, ...)/2
end for
for iface $\leftarrow 1$, nface **do**
  [P_{011},...] $\leftarrow$ getpts(P_{200}, ..., Δ^*_{011}, ...)
end for

Algorithm 3 Edge-centered offset, function getoffset011

Input: P_{200},..., P_{011},...
$\mathcal{M} \leftarrow$ metric($\frac{1}{4}(P_{020} + 2P_{011} + P_{002})$)
$\mathcal{J}_K \leftarrow$ jacobianMatrix(P_{200},...,P_{011},...)(0, 1/2, 1/2)
[R,λ] $\leftarrow$ rotScal($\mathcal{M}$,$\mathcal{J}_K$)
$T^{\mathcal{M}} \leftarrow$ metTensor(R, λ)
$\Delta_{011} \leftarrow$ offset011($T^{\mathcal{M}}$)

Algorithm 4 Element-centered offsets, function getoffsets

Input: P_{200},..., P_{011},...
$\mathcal{J}_K \leftarrow$ jacobianMatrix(P_{200},...,P_{011},...)(1/3, 1/3, 1/3)
[R,λ] $\leftarrow$ rotscal($\mathcal{M}$,P_{200},P_{020},P_{002})
$T^{\mathcal{M}} \leftarrow$ mettensor(R, λ)
$[\Delta_{011}, \Delta_{101}, \Delta_{110}] \leftarrow$ offsets($T^{\mathcal{M}}$)

Figures 4 and 5 show, respectively, the edge and element centered results on the coarse mesh. Figures 6 and 7 on the fine mesh, in the same order. The mesh is of the unit square $[0.1, 1.1]^2$, to avoid the metric field singularity at the origin. The resulting P^2 triangles are represented as well as computed gaps (thin lines). Meshes on the left are curved directly from the input linear mesh. Meshes on the right are curved using the previously curved mesh as input, corresponding to the second iteration of the fixed point algorithm.

Element curvature is visually satisfactory, in that edges seem to curve along metric field isolines. Similarly to when edge length is minimized [26], edges aligned with metric field directions associated to the smallest size tend to curved greatly, to align themselves with the highest size directions at the extremities. This behaviour is undesirable. It may be avoided by devising some curvature limiters. A possible criterion is setting an alignment threshold between control point displacement and subjacent linear edge. Another necessity is to correct the resulting meshes. Backtracking can be used while controlling for control coefficient positivity [47]. Efficient simplex-based Jacobian correction can also be used [29]. This is shown on 3D meshes to obtain the globally maximize Jacobian control coefficient minimum surrounding an edge in as little time as it takes to evaluate the control coefficients ~ 6.5 times. Constraining corrections to along the proposed displacement direction should be simple to incorporate as this method is already based on solving a linear program. More flexible constraints such as thresholds on the dot product against the displacement direction should similarly be possible to implement.

Metric field derivatives decrease with distance to the origin. As such, even on the coarse meshes, impact of a second iteration of curving is most noticeable in the bottom-left corner, closest to the origin. On the fine mesh, the effect of a second iteration is generally hard to notice, coherent with the discussion in III.C and Eq. (52). Similarly, difference between edge- and element-based curving is most noticeable where the metric field variations are the strongest, on elements closest to the origin.

In conclusion, this unit definition seems to recover the metric field's intrinsic curvature. Simple geometric equations are used, which incur minimal computational cost. Some amount of mesh correction [29, 47, 48] is necessary after the fact, especially on coarse meshes.

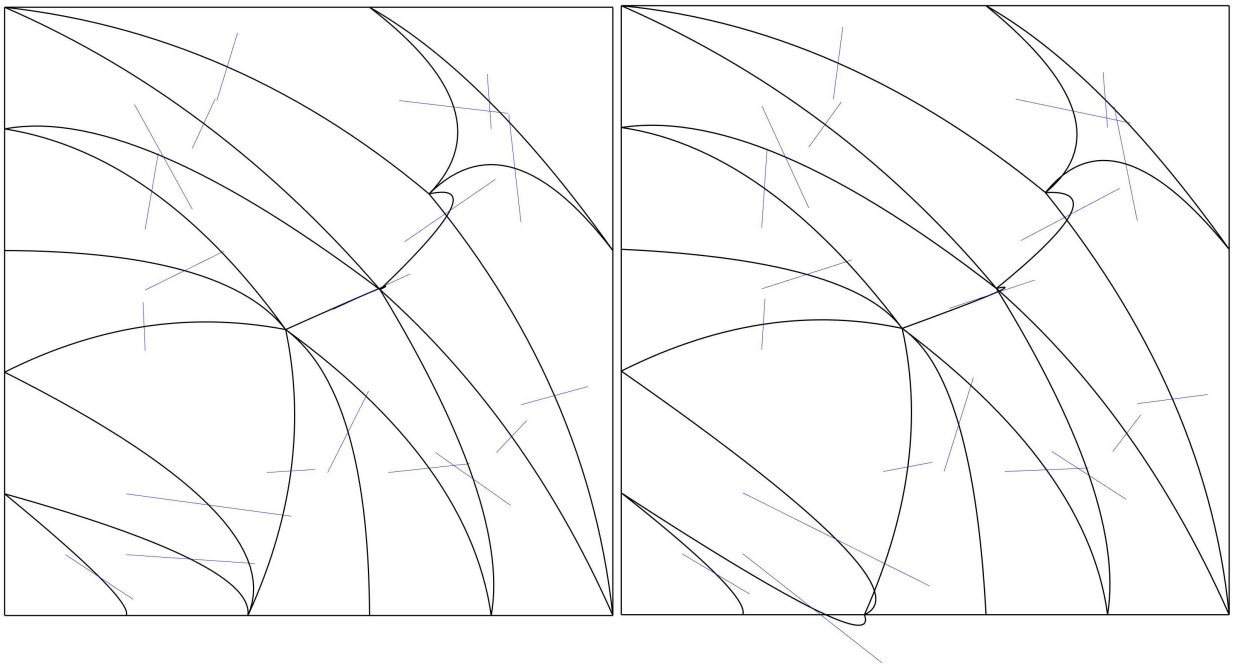

Fig. 4 First (left) and second iteration edge-centered curving on coarse mesh.

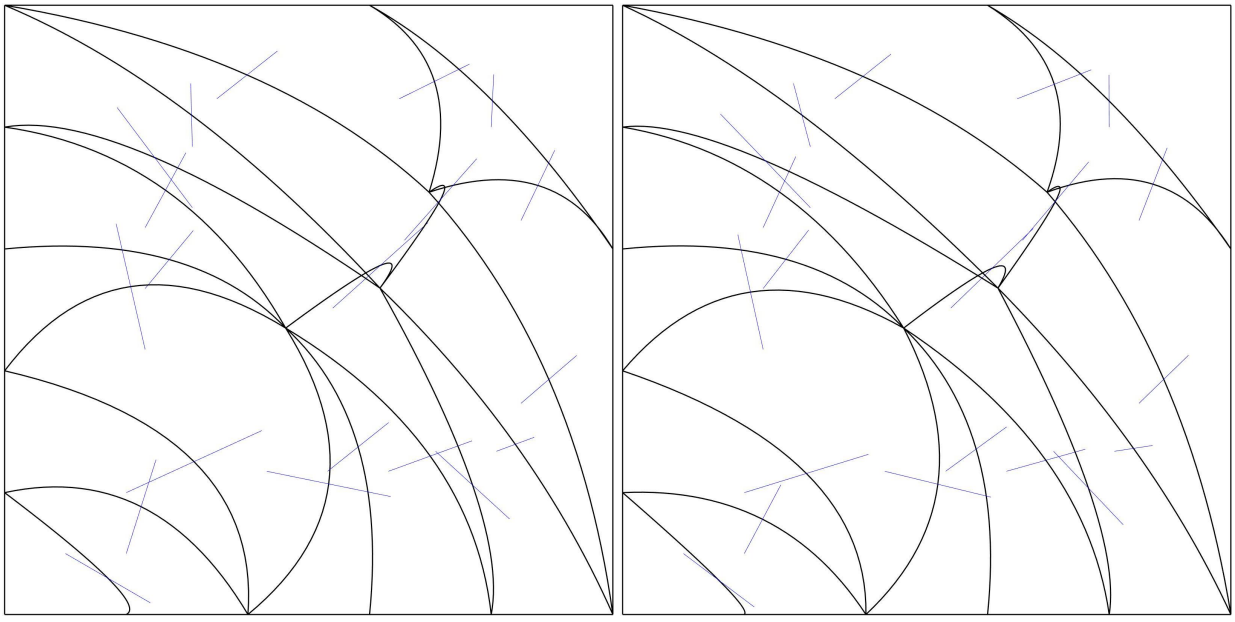

Fig. 5 First (left) and second iteration element-centered curving on coarse mesh.

V. Multi-scale error estimate on unit high-order meshes

In this Section, we present a new interpolation error estimate in L^p norm over curved elements unit in a metric field $\mathcal{M}$. The error bounds depend only on p, the interpolated function f, and the metric field $\mathcal{M}$. This is a direct generalization of the classic multi-scale error estimate [49] on linear meshes that can be used as a simple mesh adaptation driver, or to express error on a functional of interest [1]. This also offers a model of error behaviour which could be used to enrich a posteriori methods such as MOESS [3–6].

Let $f : x \in \Omega \mapsto \frac{1}{2} x^T H x$ be a quadratic function. The P^1 interpolation operator on K is denoted $\Pi_K : \Omega \to \mathbb{R}$. It is

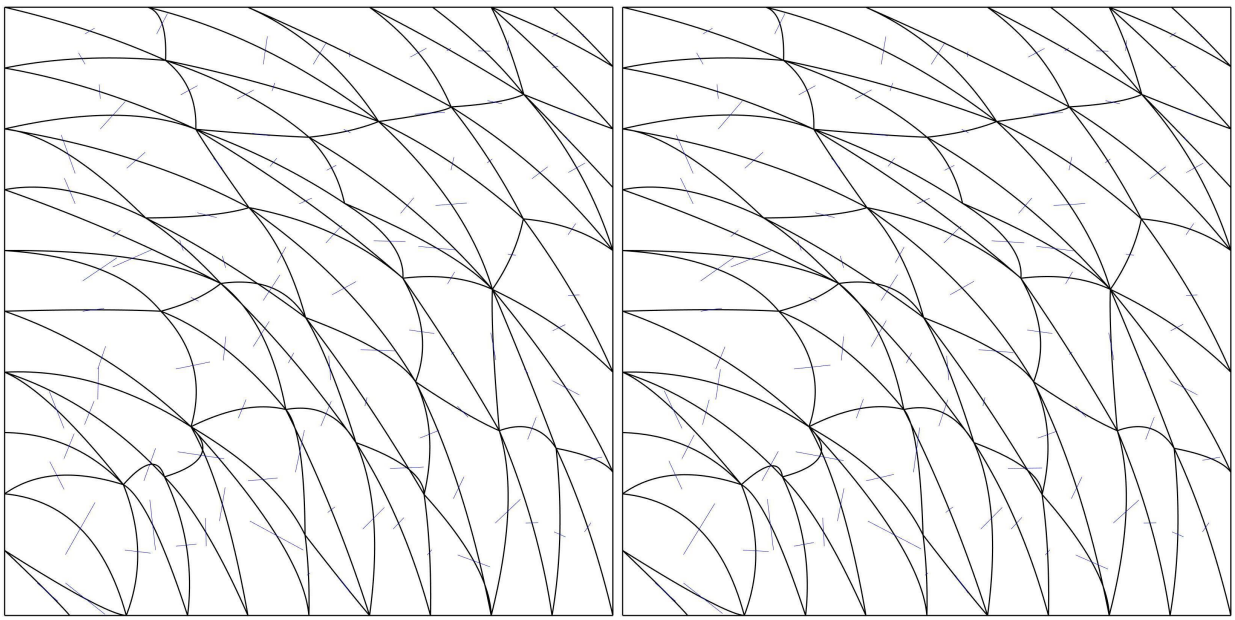

Fig. 6 First (left) and second iteration edge-centered curving on coarse mesh.

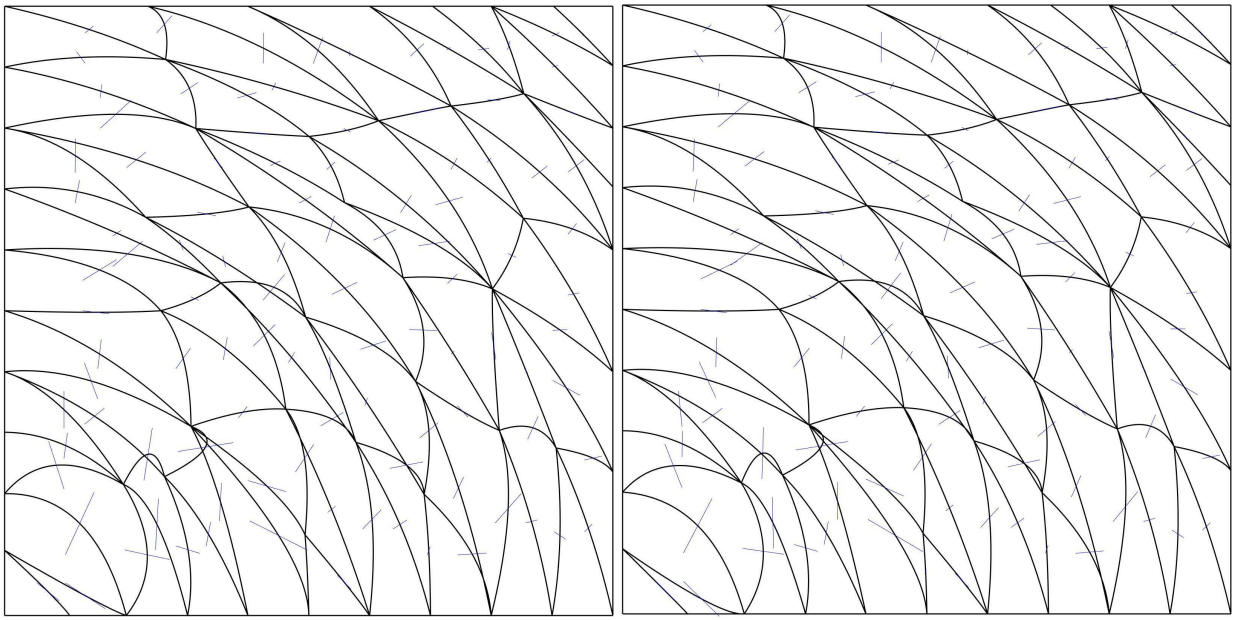

Fig. 7 First (left) and second iteration element-centered curving on fine mesh.

defined by

$$\Pi_K f = \Pi_{\widehat{K}}(f \circ F_K) \circ F_K^{-1}. \tag{69}$$

The interpolation error is $e_K f = f - \Pi_K f$. Clearly, $e_K f = e_{\widehat{K}}(f \circ F_K) \circ F_K^{-1}$. Moreover,

$$\|e_K f\|^p_{L^p(K)} = \int_K |e_K f|^p dk = \int_{\widehat{K}} |e_K f \circ F_K|^p J_K d\widehat{k}. \tag{70}$$

As such, the quantity of interest is $(e_K f) \circ F_K$, which is also $e_{\widehat{K}}(f \circ F_K)$. In other words, studying interpolation error of f on K is equivalent to studying interpolation error of $f \circ F_K$ on the reference element $\widehat{K}$. Alternatively, we can choose a regular element K_0 instead of $\widehat{K}$, and thus study $e_{K_0}(f \circ F_{K_0 \to K})$ instead.

Now, K_0 is a linear element. Thus, it is unit in a constant metric field, and this is the same as in the linear framework as shown in III.C. Its intrinsic metric is thus the identity matrix. Thus [49], denoting $f_0 = f \circ F_{K_0 \to K}$:

$$|e_{K_0} f_0(x)| \leq C \mathrm{tr}\left(\mathcal{M}_{K_0}^{-1/2}(x)|H_{f_0}(x)|\mathcal{M}_{K_0}^{-1/2}(x)\right) + O(h^3) \leq C \mathrm{tr}\left(|H_{f_0}(x)|\right) + O(h^3). \tag{71}$$

To obtain the $O(h^3)$, it suffice to expand f_0 to the third order, and recall second derivatives of the element mapping are a $O(h^2)$. Denoting $I_K = F_{K_0 \to K}$, the Hessian H_{f_0} is comprised of the entries:

$$\partial_{ij} f_0 = \sum_s \partial_{ij} I_K^{(s)} \partial_s f(I_K) + \sum_{st} \partial_i I_K^{(s)} \partial_j I_K^{(t)} \partial_{st} f(I_K) \tag{72}$$

Let us introduce $\mathcal{M}$ the unique metric in which K is unit. The second derivatives become:

$$\partial_{ij} f_0 = \sum_{stu} (R_{tj} R_{ui} + R_{uj} R_{ti}) T^{\mathcal{M}}_{tus} \partial_s f(I_K) + \sum_{st} (\mathcal{M}^{-1/2} R)_{si} (\mathcal{M}^{-1/2} R)_{tj} \partial_{st} f(I_K) + O(h^3) \tag{73}$$

This now depends only on $\mathcal{M}$, no longer K, save for through R. The $O(h^3)$ is a consequence of the consistency shown at III.C.

Let us detail in the case where H_{f_0} is positive definite. The matrix defined by the second sum is positive definite if f is strictly convex. For $\|\nabla f\|/\|H\|$ small enough, for instance, the total Hessian is positive definite. In this case, $|H_{f_0}| = H_{f_0}$ thus

$$\mathrm{tr}\left(|H_{f_0}|\right) = 2 \sum_{istu} R_{ti} R_{ui} T^{\mathcal{M}}_{tus} \partial_s f(I_K) + \sum_{ist} (\mathcal{M}^{-1/2} R)_{si} (\mathcal{M}^{-1/2} R)_{ti} \partial_{st} f(I_K) \tag{74}$$

Now $\sum_i R_{ti} R_{ui} = (R^T R)_{ut} = \delta_{ut}$ thus

$$2 \sum_{istu} R_{ti} R_{ui} T^{\mathcal{M}}_{tus} \partial_s f(I_K) = 2 \sum_{st} T^{\mathcal{M}}_{tts} \partial_s f(I_K) \tag{75}$$

As previously mentioned, writing in terms of the mapping from the ideal rather than reference element can offer quick simplification of R. This is important because R is the only thing particularizing K with respect to other elements unit in $\mathcal{M}$. Symmetry of $T^{\mathcal{M}}$ (metric derivatives symmetry condition) can be used to write this slightly more compactly as $\sum_t (T^{\mathcal{M}} \times_1 \partial f)_{tt}$. As for the second sum, it is simply

$$\sum_i (\mathcal{M}^{-1/2} R)^T H_f (\mathcal{M}^{-1/2} R) = \mathrm{tr}\left(R^T \mathcal{M}^{-1/2} H_f \mathcal{M}^{-1/2} R\right) = \mathrm{tr}\left(\mathcal{M}^{-1/2} H_f \mathcal{M}^{-1/2}\right) \tag{76}$$

where R also simplifies. In conclusion, interpolation error is majored pointwise on the ideal element K_0 by

$$|e_{K_0} f_0(x)| \leq C \left(2 \sum_t (T^{\mathcal{M}}(x) \times_1 \partial f(x))_{tt} + \mathrm{tr}\left(\mathcal{M}^{-1/2}(x) H_f(x) \mathcal{M}^{-1/2}(x)\right)\right). \tag{77}$$

Now the L^p norm over K is

$$\begin{aligned} \int_K |e_K f(x)|^p dk = \int_K |e_K f(x)|^p dk = \int_{K_0} \det(\mathcal{M}^{-1/2}) |e_{K_0} f_0(x)|^p dk \\ \leq C \int_{K_0} \det(\mathcal{M}^{-1/2}(x)) \left(2 \sum_t (T^{\mathcal{M}}(x) \times_1 \partial f(x))_{tt} + \mathrm{tr}\left(\mathcal{M}^{-1/2}(x) H_f(x) \mathcal{M}^{-1/2}(x)\right)\right) dk \end{aligned} \tag{78}$$

where the Jacobian matrix determinant has been substituted using element unitness.

This canonical estimator illustrates the fact the metric fields define appropriately small reference classes of high-order unit elements, as the parameter particularizing K in its class (the rotation matrix R) has been simplified away, with no need for brutal majoration. If the metric field is piece-wise constant as on a straight mesh, $T^{\mathcal{M}}$ vanishes, thus we obtain again the classic multi-scale estimator [49]. Otherwise, there are new terms to take into account, that depend on metric field derivatives.

VI. Conclusion

This paper introduces a generalization of the unit mesh definition to high-order elements. We illustrate its ability to curve mesh elements to capture metric implied curvature, and to account for higher-order element mapping terms in a continuous context (involving only a metric field). We begin with a discrete relationship between a polynomial metric field and quadratic element, and deduce necessary and sufficient conditions on the mapping Jacobian and second derivatives, in terms of the metric field. These conditions form a fixed point problem shown to converge very fast (in terms of mesh size h) thus of which a single iteration from a straight mesh may be sufficient for practical purposes. We illustrate the resulting curving procedure on a simple case with an analytical metric field. The meshes are shown to curve along dominant metric directions naturally.

A constraint on metric field derivatives has become necessary, either to guarantee mapping Hessian symmetry if departing straight from a Jacobian based definition $\mathcal{J}_K \sim \mathcal{M}^{-1/2}\mathcal{J}_0$, or to guarantee element-implied metric uniqueness if departing from the "zeroth order" definition $F_K \sim \mathcal{M}^{-1/2}F_0$. As our analysis proceeded from the "zeroth order" definition, geometric relationships were naturally "symmetrized", i.e. it has not proven necessary to assume this constraint until the element-implied metric has been sought. This means it is possible to curve meshes using a metric field that does not respect these symmetry conditions. In fact, the numerical example uses such a metric field.

Meshes unit in a family of embedded metric fields are proved to become straighter, at the rate shown to preserve classic convergence rate estimates [19]. This asymptotic analysis also allows us to recast the definition in a fully continuous setting. This fully continuous setting is used to produce an example error estimate, by allowing element dependent quantities be rewritten immediately in terms of the implied metric field. The considered estimator generalizes the classic multi-scale L^p norm of P^1 interpolation error estimator to curved meshes, and now involves metric field derivatives explicitly. Through these example applications, in meshing (curving) and error estimation, we believe the potential of this approach as a basis for high-order metric-based adaptation has been illustrated. The analysis leading to these results is very simple and should extend trivially to higher-order elements, at the cost perhaps of additional constraints on the metric field (symmetry of higher-order derivative tensors).

Future work Topological triggers and operations need to be devised based on this unit mesh definition. Edge-based operations are particularly efficient for linear meshing [33–36], and similar strategies need to be devised for high-order elements with the proposed generalized definition. A starting point may be to notice the first order unit relationship implies the Bézier control net elements should be unit as linear elements.

Integrating the metric field derivatives tensor involved in the multi-scale estimator to MOESS could provide a posteriori error estimation that better takes into account metric field induced curvature. This requires computing the mesh-implied metric field, which is provided here. Similarly, the multi-scale estimator may perhaps be minimized analytically similarly to the linear case, in order to investigate the impact of curvature on the optimal metric field produced.

The multi-scale error estimator is provided as an application example of this unit definition. It shows how metric curvature (through its derivatives) is naturally taken into account. However, it concerns only P^1 interpolation, which is not useful in a practical context. At least P^2 interpolation error needs to be addressed. It suffices to collect the dominant terms in $f \circ F_K$ with f cubic, but these involve second derivatives of the metric field. It is thus necessary to investigate what conditions on the metric field arise when differentiating the unit relationship twice (or similarly, considering a quadratic $\mathcal{M}^{-1/2}$, as such conditions may translate to simplifications of the interpolation error.

The symmetry constraint on the metric field derivatives needs to be investigated further. Some kind of (probably Riemannian) geometric interpretation could help better understand the implications of this constraint. When considering elements of degree above 2, it is possible similar constraints will appear involving higher-order derivatives, but it is also possible the first constraint implies the following constraints. The scope of the constraint also needs to be studied further. It is never taken into account when deriving geometric relations from the "zeroth-order" unit relationship $F_K \sim \mathcal{M}^{-1/2}F_0$. Thus, for a metric-based remesher, it may not even be necessary to dictate the input metric field, or rather the metric interpolation scheme, respects this condition.

Appendix

A. Metric derivatives symmetry condition

Assume a high-order element K verifies:

$$\forall \xi, \partial F_K^T(\xi) = \mathcal{M}^{-1/2}(F_K(\xi)) R \partial F_0^T.$$

Let us simplify by assuming K_0 was chosen for R to be identity, and omit function evaluations. This rewrites, for all i, k,

$$\partial_i F_K^k = (\mathcal{M}^{-1/2} \partial F_0^T)_{ki} = \sum_s \partial_i F_0^s \mathcal{M}_{ks}^{-1/2}$$

Then the second derivatives: for all i, j, k,

$$\begin{aligned}\partial_{ij} F_K^k = \partial_j \sum_s \partial_i F_0^s \mathcal{M}_{ks}^{-1/2} &= \sum_s \partial_{ij} F_0^s \mathcal{M}_{ks}^{-1/2} + \sum_s \partial_i F_0^s \partial_j \mathcal{M}_{ks}^{-1/2} \circ F_K \\ &= \sum_{st} \partial_i F_0^s \partial_j F_K^t \partial_t \mathcal{M}_{ks}^{-1/2}\end{aligned}$$

Lastly, we can replace $\partial_j F_K^t$ using the first relationship:

$$\partial_{ij} F_K^k = \sum_{stu} \partial_i F_0^s \partial_j F_0^u \mathcal{M}_{tu}^{-1/2} \partial_t \mathcal{M}_{ks}^{-1/2}.$$

The left-hand side is symmetric in that, for all k and i, j, $\partial_{ij} F_K^k = \partial_{ji} F_K^k$. The right-hand side is only symmetric if

$$\forall k, s, u, \ \sum_t \mathcal{M}_{tu}^{-1/2} \partial_t \mathcal{M}_{ks}^{-1/2} - \mathcal{M}_{ts}^{-1/2} \partial_t \mathcal{M}_{ku}^{-1/2} = 0.$$

B. P^2 geometric relationships, computational details

Recall the basic relationships. For all ξ,

$$\begin{aligned}\partial F_K^T(\xi_0)(\xi - \xi_0) &= \mathcal{M}^{-1/2} R \partial F_0^T (\xi - \xi_0) \\ \text{and} \quad \frac{1}{2} \sum_{st} (\xi - \xi_0)_s (\xi - \xi_0)_t \partial_{st} F_K(\xi_0) &= \left[T \times_1 (\xi - \xi_0)\right] R \partial F_0^T (\xi - \xi_0).\end{aligned}$$

We can identify polynomial coefficients in the first equation, yielding a first-order unit condition:

$$\partial F_K^T(\xi_0) = \mathcal{M}^{-1/2}(F_K(\xi_0)) R \partial F_0^T \tag{79}$$

This is the definition of a unit linear element.

We now seek to identify polynomial coefficients in the second relationship. To identify successive products against $\xi - \xi_0$ is a pitfall. The left-hand side will, of course, be symmetric, but the right-hand side will not. The problem is some P^2 terms of $\xi - \xi_0$ are repeated on the left-hand side, whereas they are multiplicated to unique terms on the right-hand side. Let us denote $N = R \partial F_0^T$ for ease of notation. The right-hand side expands to:

$$\begin{aligned}\left(\left[T \times_1 (\xi - \xi_0)\right] N(\xi - \xi_0)\right)_i = \sum_s \left(\left[T \times_1 (\xi - \xi_0)\right] N\right)_{is} (\xi - \xi_0)_s &= \sum_{su} \left[T \times_1 (\xi - \xi_0)\right]_{iu} N_{us} (\xi - \xi_0)_s \\ &= \sum_{stu} T_{tiu} N_{us} (\xi - \xi_0)_s (\xi - \xi_0)_t\end{aligned}$$

We can then identify the diagonal and extra-diagonal components of $\partial^2 F_K^k$

$$\frac{1}{2} \partial_{ii} F_K^k = \sum_s T_{iks}^{\mathcal{M}} N_{si} \quad \text{and} \quad \partial_{ij} F_K^k = \sum_s T_{iks}^{\mathcal{M}} N_{sj} + T_{jks}^{\mathcal{M}} N_{si}$$

or simply:

$$\forall (i,j,k),\ \partial_{ij} F_K^k = \sum_s (T_{iks} N_{sj} + T_{jks} N_{si}).$$

The tensor $T = \partial F_K(\xi_0) \times_1 \partial \mathcal{M}^{-1/2}$ can be rewritten by injecting the first-order unit conditon Eq. (79):

$$T = \partial F_K(\xi_0) \times_1 \partial \mathcal{M}^{-1/2} = (N^T \mathcal{M}^{-1/2}) \times_1 \partial \mathcal{M}^{-1/2} = N^T \times_1 T^{\mathcal{M}}$$

with $T^{\mathcal{M}} = \mathcal{M}^{-1/2}(F_K(\xi_0)) \times_1 \partial \mathcal{M}^{-1/2}(F_K(\xi_0))$. Thus

$$\partial_{ij} F_K^k = \sum_{st} (N_{ti} N_{sj} + N_{tj} N_{si}) T^{\mathcal{M}}_{tks}.$$

The right-hand side is appropriately symmetric for arbitrary $\mathcal{M}$. Note, the left-hand side is constant.

C. Circular metric derivations

We provide the tensor associated to the analytical metric field used in Section IV.F for ease of reproduction. Let us compute the derivatives of $M = \mathcal{M}^{-1/2}$:

$$(\partial M \circ \phi)_{ijk} = \sum_s \partial_i \phi_s \partial_s M_{jk} = \partial\phi \partial M_{jk}$$

Thus, for all j,k, $\partial M_{jk} = (\partial\phi)^{-1} \partial (M_{jk} \circ \phi)$. The Jacobian is given by :

$$\partial\phi(r,\theta) = \begin{pmatrix} \cos\theta & \sin\theta \\ -r\sin\theta & r\cos\theta \end{pmatrix}$$

of inverse:

$$\partial\phi^{-1}(r,\theta) = \frac{1}{r}\begin{pmatrix} r\cos\theta & -\sin\theta \\ r\sin\theta & \cos\theta \end{pmatrix}$$

The metric writes:

$$M = \begin{pmatrix} R_{11}^2 h_1 + R_{12}^2 h_2 & R_{21}R_{11}h_1 + R_{22}R_{12}h_2 \\ \star & R_{21}^2 h_1 + R_{22}^2 h_2 \end{pmatrix}$$

thus:

$$\partial M_{11} \circ \phi = 2(R_{11}\partial R_{11} h_1 + R_{12}\partial R_{12} h_2) = \begin{pmatrix} 0 \\ 2\cos\theta\sin\theta(h_2 - h_1) \end{pmatrix}$$

$$\partial M_{21} \circ \phi = (R_{21}\partial R_{11} + \partial R_{21} R_{11})h_1 + (R_{22}\partial R_{12} + \partial R_{22} R_{12})h_2) = \begin{pmatrix} 0 \\ (-\sin^2\theta + \cos^2\theta)(h_1 - h_2) \end{pmatrix}$$

$$\partial M_{22} \circ \phi = 2(R_{21}\partial R_{21} h_1 + R_{22}\partial R_{22} h_2) = \begin{pmatrix} 0 \\ 2\cos\theta\sin\theta(h_1 - h_2) \end{pmatrix}$$

Then,

$$\partial M_{11} = \frac{2\cos\theta\sin\theta(h_1 - h_2)}{r}\begin{pmatrix} \sin\theta \\ -\cos\theta \end{pmatrix}, \quad \partial M_{21} = \frac{(-\sin^2\theta + \cos^2\theta)(h_1 - h_2)}{r}\begin{pmatrix} -\sin\theta \\ \cos\theta \end{pmatrix}$$

$$\partial M_{22} = \frac{2\cos\theta\sin\theta(h_1 - h_2)}{r}\begin{pmatrix} -\sin\theta \\ \cos\theta \end{pmatrix}$$

Finally, let us compute $T^{\mathcal{M}}_{ijk} = \sum_s M_{is}(\partial M)_{sjk}$:

$$T^{\mathcal{M}}_{111} = M_{11}\partial_1 M_{11} + M_{12}\partial_2 M_{11} = \frac{2\cos\theta\sin\theta(h_1 - h_2)}{r}\left(\sin\theta(R_{11}^2 h_1 + R_{12}^2 h_2) - \cos\theta(R_{21}R_{11}h_1 + R_{22}R_{12}h_2)\right)$$

$$T^{\mathcal{M}}_{211} = M_{21}\partial_1 M_{11} + M_{22}\partial_2 M_{11} = \frac{2\cos\theta\sin\theta(h_1 - h_2)}{r}\left(\sin\theta(R_{21}R_{11}h_1 + R_{22}R_{12}h_2) - \cos\theta(R_{21}^2 h_1 + R_{22}^2 h_2)\right)$$

and

$$T^{\mathcal{M}}_{112} = M_{11}\partial_1 M_{12} + M_{12}\partial_2 M_{12} = \frac{(-\sin^2\theta + \cos^2\theta)(h_1 - h_2)}{r}\left(-\sin\theta(R^2_{11}h_1 + R^2_{12}h_2) + \cos\theta(R_{21}R_{11}h_1 + R_{22}R_{12}h_2)\right)$$

$$T^{\mathcal{M}}_{212} = M_{21}\partial_1 M_{12} + M_{22}\partial_2 M_{12} = \frac{(-\sin^2\theta + \cos^2\theta)(h_1 - h_2)}{r}\left(-\sin\theta(R_{21}R_{11}h_1 + R_{22}R_{12}h_2) + \cos\theta(R^2_{21}h_1 + R^2_{22}h_2)\right)$$

and

$$T^{\mathcal{M}}_{122} = M_{11}\partial_1 M_{22} + M_{12}\partial_2 M_{22} = \frac{2\cos\theta\sin\theta(h_1 - h_2)}{r}\left(-\sin\theta(R^2_{11}h_1 + R^2_{12}h_2) + \cos\theta(R_{21}R_{11}h_1 + R_{22}R_{12}h_2)\right)$$

$$T^{\mathcal{M}}_{222} = M_{21}\partial_1 M_{22} + M_{22}\partial_2 M_{22} = \frac{2\cos\theta\sin\theta(h_1 - h_2)}{r}\left(-\sin\theta(R_{21}R_{11}h_1 + R_{22}R_{12}h_2) + \cos\theta(R^2_{21}h_1 + R^2_{22}h_2)\right)$$

Acknowledgments

This work was funded by the EnCAPS project, AFRL Contract FA8650–20–2–2002: "EnCAPS: Enhanced Computational Aircraft Prototype Syntheses", with Dr. Richard Snyder as the Technical Monitor. Funding was also provided by Oak Ridge National Laboratories under DOE Contract 4000192102 with Dr. Ryan Glasby as the Technical Monitor.

References

[1] Alauzet, F., and Frazza, L., "Feature-based and goal-oriented anisotropic mesh adaptation for RANS applications in aeronautics and aerospace," *Journal of Computational Physics*, Vol. 439, 2021, p. 110340. https://doi.org/10.1016/j.jcp.2021.110340.

[2] Loseille, A., and Alauzet, F., "Continuous mesh framework part I: well-posed continuous interpolation error," *SIAM Journal on Numerical Analysis*, Vol. 49, No. 1, 2011, pp. 38–60. https://doi.org/10.1137/090754078.

[3] Yano, M., and Darmofal, D. L., "An Optimization-Based Framework for Anisotropic Simplex Mesh Adaptation," *Journal of Computational Physics*, Vol. 231, No. 22, 2012, pp. 7626–7649. https://doi.org/10.1016/j.jcp.2012.06.040.

[4] Carson, H. A., Huang, A. C., Galbraith, M. C., Allmaras, S. R., and Darmofal, D. L., "Anisotropic mesh adaptation for continuous finite element discretization through mesh optimization via error sampling and synthesis," *Journal of Computational Physics*, Vol. 420, 2020, p. 109620. https://doi.org/10.1016/j.jcp.2020.109620.

[5] Carson, H. A., Huang, A. C., Galbraith, M. C., Allmaras, S. R., and Darmofal, D. L., "Mesh optimization via error sampling and synthesis: An update," AIAA 2020–0087, January 2020. https://doi.org/10.2514/6.2020-0087.

[6] Carson, H. A., "Provably Convergent Anisotropic Output-Based Adaptation for Continuous Finite Element Discretizations," PhD thesis, Massachusetts Institute of Technology, Department of Aeronautics and Astronautics, Nov. 2019.

[7] Loseille, A., "Anisotropic 3D Hessian-based multi-scale and adjoint-based mesh adaptation for Computational Fluid Dynamics: Application to high fidelity sonic boom prediction." Theses, Université Pierre et Marie Curie - Paris VI, Dec. 2008.

[8] Loseille, A., Menier, V., and Alauzet, F., "Parallel generation of large-size adapted meshes," *Procedia Engineering*, Vol. 124, 2015, pp. 57–69.

[9] Alauzet, F., and Loseille, A., "High-order sonic boom modeling based on adaptive methods," *Journal of Computational Physics*, Vol. 229, No. 3, 2010, pp. 561–593. https://doi.org/10.1016/j.jcp.2009.09.020.

[10] Michal, T., Krakos, J., Kamenetskiy, D., Galbraith, M., Ursachi, C.-I., Park, M. A., Anderson, W. K., Alauzet, F., and Loseille, A., "Comparing Unstructured Adaptive Mesh Solutions for the High Lift Common Research Airfoil," *AIAA Journal*, Vol. 59, No. 9, 2021, pp. 3566–3584.

[11] Alauzet, F., Loseille, A., Marcum, D., and Michal, T. R., "Assessment of anisotropic mesh adaptation for high-lift prediction of the HL-CRM configuration," *23rd AIAA Computational Fluid Dynamics Conference*, 2017, p. 3300. https://doi.org/10.2514/6.2017-3300.

[12] Alauzet, F., Clerici, F., Loseille, A., Maunoury, M., Rochery, L., Tarsia-Morisco, C., Tenkes, L.-M., and Vanharen, J., "4th AIAA CFD High Lift Prediction Workshop results using metric-based anisotropic mesh adaptation," *AIAA Aviation 2022 Forum*, 2022, p. 3521. https://doi.org/10.2514/6.2022-3521.

[13] Coulaud, O., and Loseille, A., "Very High Order Anisotropic Metric-Based Mesh Adaptation in 3D," *Procedia Engineering*, Vol. 163, 2016, pp. 353 – 365. https://doi.org/10.1016/j.proeng.2016.11.071, 25th International Meshing Roundtable.

[14] Ergatoudis, I., Irons, B. M., and Zienkiewicz, O. C., "Curved, isoparametric, 'quadrilateral' elements for finite element analysis," *International Journal of Solids and Structures*, Vol. 4, No. 1, 1968, pp. 31–42. https://doi.org/10.1016/0020-7683(68)90031-0.

[15] Ciarlet, P. G., "Isoparametric finite elements and Applications to second order problems over curved domains," *The finite element method for elliptic problems*, No. v. 4 in Studies in mathematics and its applications, North-Holland Pub. Co. ; sole distributors for the U.S.A. and Canada, Elsevier North-Holland, Amsterdam ; New York : New York, 1978, pp. 224–286.

[16] Huerta, A., Angeloski, A., Roca, X., and Peraire, J., "Efficiency of high-order elements for continuous and discontinuous Galerkin methods," *International Journal for Numerical Methods in Engineering*, Vol. 96, No. 9, 2013, pp. 529–560. https://doi.org/10.1002/nme.4547.

[17] Wang, Z., Fidkowski, K., Abgrall, R., Bassi, F., Caraeni, D., Cary, A., Deconinck, H., Hartmann, R., Hillewaert, K., Huynh, H., Kroll, N., May, G., Persson, P.-O., van Leer, B., and Visbal, M., "High-order CFD methods: current status and perspective," *International Journal for Numerical Methods in Fluids*, Vol. 72, No. 8, 2013, pp. 811–845. https://doi.org/10.1002/fld.3767, _eprint: https://onlinelibrary.wiley.com/doi/pdf/10.1002/fld.3767.

[18] Bassi, F., and Rebay, S., "High-order accurate discontinuous finite element solution of the 2D Euler equations," *Journal of Computational Physics*, Vol. 138, No. 2, 1997, pp. 251–285. https://doi.org/10.1006/jcph.1997.5454.

[19] Ciarlet, P. G., and Raviart, P.-A., "The combined effect of curved boundaries and numerical integration in isoparametric finite element methods," *The mathematical foundations of the finite element method with applications to partial differential equations*, Elsevier, 1972, pp. 409–474. https://doi.org/10.1016/B978-0-12-068650-6.50020-4.

[20] Lenoir, M., "Optimal isoparametric finite elements and error estimates for domains involving curved boundaries," *SIAM Journal on Numerical Analysis*, Vol. 23, No. 3, 1986, pp. 562–580. https://doi.org/10.1137/0723036.

[21] Zwanenburg, P., and Nadarajah, S., "On the Necessity of Superparametric Geometry Representation for Discontinuous Galerkin Methods on Domains with Curved Boundaries," *23rd AIAA Computational Fluid Dynamics Conference*, 2017.

[22] Moxey, D., Sastry, S. P., and Kirby, R. M., "Interpolation error bounds for curvilinear finite elements and their implications on adaptive mesh refinement," *Journal of Scientific Computing*, Vol. 78, No. 2, 2019, pp. 1045–1062.

[23] Botti, L., "Influence of Reference-to-Physical Frame Mappings on Approximation Properties of Discontinuous Piecewise Polynomial Spaces," *Journal of Scientific Computing*, Vol. 52, 2012. https://doi.org/10.1007/s10915-011-9566-3.

[24] Docampo-Sánchez, J., Ruiz-Gironés, E., and Roca, X., "An Efficient Solver to Approximate CAD Curves with Super-Convergent Rates," , 2022. https://doi.org/https://doi.org/10.5281/zenodo.6562447.

[25] Sanjaya, D. P., and Fidkowski, K., "High-Order Node Movement Discretization Error Control in Shape Optimization," *AIAA SCITECH 2023 Forum*, 2023, p. 2367.

[26] Rochery, L., "Adaptation courbe de maillages sous champ de métriques anisotropes," PhD Thesis, Inria Saclay - Université Paris-Saclay, 2023.

[27] Zhang, R., Johnen, A., and Remacle, J.-F., "Curvilinear mesh adaptation," *International Meshing Roundtable*, Springer, 2018, pp. 57–69.

[28] Bawin, A., Garon, A., and Remacle, J.-F., "Optimally convergent isoparametric P2 mesh generation," *International Meshing Roundtable*, Springer, 2018.

[29] Rochery, L., and Loseille, A., "Fast High-Order Mesh Correction for Metric-Based Cavity Remeshing and a Posteriori Curving of P2 Tetrahedral Meshes," *Computer-Aided Design*, Vol. 163, 2023, p. 103575. https://doi.org/https://doi.org/10.1016/j.cad.2023.103575.

[30] Aparicio-Estrems, G., Gargallo-Peiró, A., and Roca, X., "High-Order Metric Interpolation for Curved R-Adaption by Distortion Minimization," *SIAM International Meshing Roundtable*, Zenodo, 2022. https://doi.org/10.5281/zenodo.6562456.

[31] Sanjaya, D., "Towards Automated, Metric-Conforming, Mesh Optimization for High-Order, Finite-Element Methods," PhD Thesis, 2019.

[32] Ciarlet, P. G., and Raviart, P.-A., "Interpolation theory over curved elements, with applications to finite element methods," *Computer Methods in Applied Mechanics and Engineering*, Vol. 1, No. 2, 1972, pp. 217–249.

[33] Dompierre, J., Vallet, M.-G., Bourgault, Y., Fortin, M., and Habashi, W. G., "Anisotropic mesh adaptation: towards user-independent, mesh-independent and solver-independent CFD. Part III. Unstructured meshes," *International Journal for Numerical Methods in Fluids*, Vol. 39, No. 8, 2002, pp. 675–702. https://doi.org/10.1002/fld.357.

[34] Coupez, T., Jannoun, G., Veysset, J., and Hachem, E., *Edge-Based Anisotropic Mesh Adaptation for CFD Applications*, Springer Berlin Heidelberg, Berlin, Heidelberg, 2013, pp. 567–583. https://doi.org/10.1007/978-3-642-33573-0_33.

[35] Loseille, A., *Recent Improvements on Cavity-Based Operators for RANS Mesh Adaptation*, 2018. https://doi.org/10.2514/6.2018-0922.

[36] Michal, T., and Krakos, J., "Anisotropic mesh adaptation through edge primitive operations," AIAA 2012–159, January 2012. https://doi.org/10.2514/6.2012-159.

[37] Dompierre, J., Vallet, M. G., Labbé, P., and Guibault, F., "An analysis of simplex shape measures for anisotropic meshes," *Computer Methods in Applied Mechanics and Engineering*, Vol. 194, No. 48, 2005, pp. 4895–4914. https://doi.org/10.1016/j.cma.2004.11.018.

[38] Chen, L., "Mesh Smoothing Schemes Based On Optimal Delaunay Triangulations," *13th International Meshing Roundtable*, 2004, pp. 109–120.

[39] Amari, T., Canou, A., Aly, J.-J., Delyon, F., and Alauzet, F., "Magnetic cage and rope as the key for solar eruptions," *Nature*, Vol. 554, 2018, pp. 211–215. https://doi.org/10.1038/nature24671.

[40] Frey, P.-J., and Alauzet, F., "Anisotropic mesh adaptation for CFD computations," *Computer Methods in Applied Mechanics and Engineering*, Vol. 194, No. 48-49, 2005, pp. 5068–5082. https://doi.org/10.1016/j.cma.2004.11.025.

[41] Carson, H. A., Huang, A. C., Galbraith, M. C., Allmaras, S. R., and Darmofal, D. L., "Mesh Optimization via Error Sampling and Synthesis: An Update," *AIAA SciTech 2020 Forum*, American Institute of Aeronautics and Astronautics, Orlando, FL, 2020. https://doi.org/10.2514/6.2020-0087.

[42] Loseille, A., Dervieux, A., and Alauzet, F., "Fully anisotropic goal-oriented mesh adaptation for 3D steady Euler equations," *Journal of Computational Physics*, Vol. 229, No. 8, 2010, pp. 2866 – 2897. https://doi.org/10.1016/j.jcp.2009.12.021.

[43] Ciarlet, P. G., *The finite element method for elliptic problems*, SIAM, 2002.

[44] Loseille, A., and Rochery, L., "Developments on the P2 cavity operator and Bézier Jacobian correction using the simplex algorithm." *AIAA SciTech 2022 Forum*, 2022, p. 0389. https://doi.org/10.2514/6.2022-0389.

[45] Aparicio-Estrems, G., Gargallo-Peiró, A., and Roca, X., "Combining High-Order Metric Interpolation and Geometry Implicitization for Curved r-Adaption," *Computer-Aided Design*, Vol. 157, 2023, p. 103478. https://doi.org/https://doi.org/10.1016/j.cad.2023.103478.

[46] Galbraith, M. C., Allmaras, S. R., and Darmofal, D. L., "A verification driven process for rapid development of CFD software," AIAA 2015-0818, January 2015. https://doi.org/10.2514/6.2015-0818.

[47] George, P.-L., and Borouchaki, H., "Construction of tetrahedral meshes of degree two," *International Journal for Numerical Methods in Engineering*, Vol. 90, No. 9, 2012, pp. 1156–1182. https://doi.org/10.1002/nme.3364.

[48] Toulorge, T., Geuzaine, C., Remacle, J.-F., and Lambrechts, J., "Robust untangling of curvilinear meshes," *Journal of Computational Physics*, Vol. 254, 2013, pp. 8 – 26.

[49] Loseille, A., and Alauzet, F., "Optimal 3D highly anisotropic mesh adaptation based on the continuous mesh framework," *Proceedings of the 18th International Meshing Roundtable*, Springer, 2009, pp. 575–594. https://doi.org/10.1007/978-3-642-04319-2_33.